Engineering Analysis with Boundary Elements 188 (2026) 106745

Contents lists available at ScienceDirect

Engineering Analysis with Boundary Elements

journal homepage: www.elsevier.com/locate/enganabound

Isogeometric evaluation of higher-order shear deformation theories for functionally graded magneto-electro-elastic nanoplates under nonlocal strain gradient elasticity

Chien H. Thai [a,b], P.T. Hung [c], Magd Abdel Wahab [d,e,f], P. Phung-Van [g,*]

[a] Mechanics of Advanced Materials and Structures, Institute for Advanced Study in Technology, Ton Duc Thang University, Ho Chi Minh City, Vietnam
[b] Faculty of Civil Engineering, Ton Duc Thang University, Ho Chi Minh City, Vietnam
[c] Faculty of Civil Engineering, Ho Chi Minh City University of Technology and Engineering (HCMUTE), Ho Chi Minh City, Vietnam
[d] Soete Laboratory, Department of Electrical Energy, Metals, Mechanical Constructions and Systems, Faculty of Engineering and Architecture, Ghent University, 9000 Ghent, Belgium
[e] College of Engineering, Yuan Ze University, Taoyuan City, Taiwan
[f] Parallel and Distributed Systems Laboratory, Jožef Stefan Institute, Jamova cesta 39, SI-1000, Ljubljana, Slovenia
[g] Faculty of Civil Engineering, HUTECH University, Ho Chi Minh City, Vietnam

ARTICLE INFO

Keywords:
Higher-order shear deformation theories (HSDTs)
Nonlocal strain gradient theory (NSGT)
Isogeometric analysis (IGA)
Nonlocal and strain gradient effects
Functionally graded magneto-electro-elastic (FG-MEE)

ABSTRACT

The coupled influence of higher-order shear deformation theories (HSDTs) and nonlocal strain gradient theory (NSGT) on free vibration of functionally graded magneto-electro-elastic (FG-MEE) nanoplates has not been comprehensively examined. To bridge this gap, the present study develops a unified isogeometric analysis (IGA) framework to systematically evaluate and compare three HSDTs: the four-variable C^1, five-variable C^1 and seven-variable C^0 formulations. The NSGT provides a powerful theoretical foundation for simultaneously capturing nonlocal softening and strain-gradient stiffening size effects. However, its weak-form implementation requires third- or fourth-order derivatives, which are incompatible with traditional finite element formulations when combined with the HSDTs. This limitation is overcome in the proposed approach by employing the IGA, where the high-order continuity of NURBS basis functions enables direct implementation without mixed formulations. The $C^{p\text{-}1}$ continuity of NUBRS easily satisfy the requirements for third-order and fourth-order derivatives inherent in C^0 and C^1 theories. The numerical results show two key findings. First, the HSDT choice significantly affects the frequency predictions under the NSGT with this effect becoming stronger at the nanoscale compared to classical theories. Second, softening-to-stiffening transitions depend on NSGT parameters. While, HSDT models converge to identical predictions under the pure nonlocal theory, noticeable discrepancies emerge when strain-gradient effects are incorporated, indicating that the divergence originates exclusively from the gradient contribution. Ultimately, these results highlight the importance of HSDT selection in nanoscale multi-physics modelling. The proposed unified approach provides an efficient computational tool for the accurate analysis and design optimization of MEE nanodevices.

1. Introduction

Understanding the mechanical behavior of nanostructures has become a critical research focus, which is driven by the revolutionary impact of nanotechnology across electronics, biomedicine, energy harvesting and sensors [1,2]. Nanoplates are increasingly recognized as fundamental structural components within micro- and nano-electromechanical systems (MEMS/NEMS), where they are integral to the function of actuators, resonators and sensing devices. Classical continuum mechanics fails to capture the size-dependent effects that emerge in nanostructures, which necessitates advanced theoretical frameworks to accurately predict their mechanical responses [3].

Magneto-electro-elastic (MEE) materials convert energy among mechanical, electrical and magnetic domains, which makes them ideal for sensors, actuators and energy harvesters [4,5]. Functionally graded magneto-electro-elastic (FG-MEE) structures offer enhanced design

* Corresponding author at: Faculty of Civil Engineering, HUTECH University, Ho Chi Minh City, Vietnam.
E-mail addresses: thaihoangchien@tdtu.edu.vn (C.H. Thai), pv.phuc86@hutech.edu.vn (P. Phung-Van).

https://doi.org/10.1016/j.enganabound.2026.106745
Received 18 January 2026; Received in revised form 23 March 2026; Accepted 23 March 2026
Available online 6 April 2026

flexibility and performance because their material properties vary continuously through the thickness [6]. The increasing deployment in ultra-sensitive sensors, piezoelectric nanogenerators and magnetoelectric memory devices demands accurate models accounting for both multiphysical coupling and nanoscale size effects [7].

To address classical mechanics limitations, various size-dependent theories were developed such as strain gradient theory (SGT) [8], nonlocal theory [8] and their variants [9,10]. The nonlocal strain gradient theory proposed by Lim et al. [11] unified these through two length-scale parameters, integrating both stiffness-softening (nonlocal) and stiffness-stiffening (strain gradient) effects [12]. The mathematical foundation of NSGT was recently established through intrinsic variational principles, which provided a rigorous analytical framework [13]. This advancement is crucial because nano- and micro-structured materials exhibit remarkable properties that strictly necessitate the use of suitable size-dependent theories [14,15].

Accurate nanoplate analysis requires both size-dependent theories and reliable kinematic models. Classical plate theory (CPT) is computationally efficient but ignores shear deformation, making it inaccurate for thick plates [16]. First-order shear deformation theory (FSDT) improves on this by including constant transverse shear strains, but it must use shear correction factors to compensate for its simplified stress assumption [17]. To capture more realistic shear strain distributions without requiring shear correction factors, higher-order shear deformation theories (HSDTs) have been developed [16,18–21]. A variety of HSDTs have been proposed, each balancing accuracy, computational cost and implementation complexity based on its specific formulation. A significant gap remains in the literature, as no a systematic comparative investigation has been conducted to evaluate different HSDT formulations for FG-MEE nanoplates within the NSGT framework. More importantly, a fundamental question remains unanswered: whether the shear deformation theory plays the same minor role at the nanoscale as observed in classical theories, or whether size-dependent constitutive behavior fundamentally alters the significance of these kinematic assumptions.

Researchers have extensively used nonlocal strain gradient theory along with analytical, semi-analytical and numerical methods to evaluate the size-dependent behaviors of MEE nanoplates. The literature can be broadly categorized by the plate theory applied. Some studies have employed comprehensive three-dimensional (3D) theories. Chen et al. [22] presented a 3D analytical solution for the natural frequency of FG-MEE plates. Pan et al. [23] also used a 3D elastic theory to study the bending of FG-MEE sandwich plates. Additionally, a semi-analytical solution based on 3D theory was used to analyze the static and dynamic behaviors of MEE plates [24]. A significant body of work relies on the CPT. Liu et al. [25] used the CPT for free vibration analysis and a similar solution was used to investigate plate displacement [26]. By combining the CPT with nonlocal elasticity theory, researchers analyzed the size-dependent natural frequency of rectangular [27] and circular [28] MEE nanoplates. This framework was further extended to study: vibration and buckling of double MEE nanoplates on a visco-Pasternak medium [29] and thermal vibration and buckling of porous FG-MEE nanoplates [30]. Other studies have adopted the FSDT. This theory was used with analytical solutions to analyze: large-amplitude free vibration of laminated MEE plates [35]; nonlinear bending response of MEE plates [31]; large displacement analysis of MEE plates [32]. A finite element solution combined with the FSDT was also presented for the large deformation analysis of multilayered MEE plates [33]. More advanced theories, like the HSDT, have also been widely applied. Mohammadimehr and Rostami [34] combined the HSDT with Eringen's nonlocal theory to study bending, buckling, and forced vibration. The HSDT was also combined with finite element solutions to analyze vibration in hygro-thermal environments [35] and in carbon nanotube-reinforced MEE plates [36,37]. Nonlinear analyses using the HSDT, such as Karman's geometry bending [38] and nonlinear vibration on elastic foundations [39], have also been performed. Other related models were included: sinusoidal shear deformation theory for FG-MEE nanoplates [40]; a unified nonlocal model using the HSDT for nonlinear postbuckling analysis [41]; one-variable plate theory for buckling analysis in hygro-thermal environments [42]. Finally, this research has also been extended to analyze MEE cylindrical panels and curved shells [43–46]. However, several critical gaps remain in the current literature. First, a comprehensive investigation that integrates the full NSGT with advanced HSDTs to simultaneously capture both competing size effects is still lacking. Second, no systematic comparison has quantified the influence of different HSDT formulations on the free vibration of FG-MEE plates under the NSGT. Third, the mechanisms that govern softening-stiffening transitions and their dependence on HSDT choice remain poorly understood. Finally, the role of HSDT selection at the nanoscale is not yet fully understood. Addressing these gaps carries theoretical significance for understanding the kinematic-constitutive interplay, which is essential for nanoscale mechanics and practical nanodevice design.

Combining HSDTs with the NSGT creates significant computational challenges because the NSGT weak-form requires high-order derivatives (up to 3rd or 4th order). Traditional finite element methods (FEM) with C^0 Lagrangian polynomials cannot satisfy these requirements. Other methods like mixed formulations can be used, but they are not ideal because they are complex, costly and can be unreliable. Isogeometric analysis (IGA), introduced by Hughes [47], offers an elegant solution. The IGA uses NURBS (Non-uniform rational b-splines) as basis functions, which possess inherent, controllable high-order continuity. This allows IGA to naturally satisfy the high-order derivative requirements of the NSGT without complex formulations. However, a unified IGA approach enabling seamless comparison of multiple HSDTs with different continuity requirements for FG-MEE nanoplates under the NSGT has not been developed yet. Besides, the method was later successfully extended to analyze beam [48,49], plate [21,50], and shell structures [51–53], with further development adapting it for the size-dependent behaviors of microplates (using modified couple stress theory [54,55] and modified strain gradient elasticity theory [56,57]) and nanoplates (using nonlocal elasticity theory [58–60] and the NSGT [61,62]).

The present study addresses these gaps. The primary objective is to systematically evaluate the performance of three HSDT formulations (four-variable C^1, five-variable C^1 and seven-variable C^0) for the free vibration analysis of FG-MEE nanoplates governed by the NSGT. This study develops a unified IGA approach capable of handling the complex continuity requirements of various higher-order theories. Using this tool, we exactly quantified the ways in which the choice of theory changes natural vibration predictions based on the NSGT. In addition, the analysis also clarifies the coupling between strain shear effects and size effects, while assessing influences of several parameters including the power-law index, geometry, boundary conditions and size effects on the natural frequencies of FG-MEE nanoplates. These findings demonstrate that the influence of HSDT selection is significantly amplified at the nanoscale compared to classical macroscopic theories. Consequently, the appropriate choice of the shear deformation theory acts as a pivotal determinant that governs the free vibration analysis of FG-MEE nanoplates.

2. Mathematical formulation

In this section, material properties of FG-MEE, the nonlocal strain gradient theory and NURBS basis function are presented.

2.1. Material properties

This study examines a FG-MEE nanoplate, which is illustrated in Fig. 1. The plate has a length L, width W and thickness t and is composed of Barium Titanate ($BaTiO_3$) and Cobalt Ferrite ($CoFe_2O_4$). It is subjected to both an electric potential, $\Phi(x, y, z, t)$ and a magnetic potential, $\Psi(x, y, z, t)$. To model the material, a power-law distribution is used. This calculates the material properties, which vary continuously through the plate thickness, as follows [63]

$$\widehat{P}(z) = \widehat{P}_{bo} + (\widehat{P}_{to} - \widehat{P}_{bo})V_z \tag{1}$$

where $V_z = (z/h + 0.5)^n$, $\widehat{P}$ is material properties; n is the power index; *to* and *bo* are respectively the top and bottom surfaces related to $BaTiO_3$ and $CoFe_2O_4$ materials.

2.2. Nonlocal strain gradient theory framework

According to the generated nonlocal strain gradient theory [11,12, 64], the total nonlocal stress components (t_{ij}), total electric displacement components (d_i) and total magnetic induction components (b_i) in functionally graded magneto-electro-elastic (MEE) continuum bodies are defined as

$$t_{ij}(\mathbf{x}) = \int_V \Xi(|\mathbf{x}' - \mathbf{x}|)(1 - l^2\nabla^2)\sigma_{ij}(\mathbf{x}')\mathrm{d}V(\mathbf{x}') \tag{2}$$

$$d_i(\mathbf{x}) = \int_V \Xi(|\mathbf{x}' - \mathbf{x}|)(1 - l^2\nabla^2)D_i(\mathbf{x}')\mathrm{d}V(\mathbf{x}') \tag{3}$$

$$b_i(\mathbf{x}) = \int_V \Xi(|\mathbf{x}' - \mathbf{x}|)(1 - l^2\nabla^2)B_i(\mathbf{x}')\mathrm{d}V(\mathbf{x}') \tag{4}$$

where $\Xi(|\mathbf{x}' - \mathbf{x}|)$, $\mathbf{x}$ and $\mathbf{x}'$ are the nonlocal kernel function, any point within the body and neighbor point of $\mathbf{x}$, respectively; V, l and ∇ are the volume of solid, length-scale parameter and differential operator ($\nabla = \partial/\partial x + \partial/\partial y$), respectively. The local stress (σ_{ij}), local electric displacement (D_i) and local magnetic induction (B_i) components are formulated by [35]

$$\begin{aligned} \sigma_{ij} &= c_{ijkl}\varepsilon_{kl} - e_{ijk}E_k - q_{kij}H_k \\ D_i &= e_{ikl}\varepsilon_{kl} + k_{ik}E_k + d_{ik}H_k \\ B_i &= q_{ikl}\varepsilon_{kl} + d_{ik}E_k + \mu_{ik}H_k \end{aligned} \tag{5}$$

here, the material properties c_{ij},e_{ij},q_{ij},k_{ij},d_{ij} andμ_{ij} are the coefficients for elastic stiffness, piezoelectricity, piezomagnetism, dielectric permittivity, electromagnetism and magnetic permittivity, respectively; ε_{ij}, E_i and H_i represent the strain, electric field and magnetic field components, respectively.

The motion of nonlocal MEE continuum bodies is governed by the following equations [65]

$$t_{ij,j} = \rho\ddot{u}_i \text{ in } V \tag{6}$$

$$d_{i,i} = 0 \text{ in } V \tag{7}$$

$$b_{i,i} = 0 \text{ in } V \tag{8}$$

where ρ and $\ddot{u}_i$ are the mass density and an acceleration, respectively; the symbol ",i" is the derivative of arbitrary function.

According to Eringen's nonlocal elasticity theory [66], the nonlocal kernel ($\Xi(|\mathbf{x}' - \mathbf{x}|)$) is equivalent to the Green's function of a linear differential operator L, given by [67]

$$L(\Xi(|\mathbf{x}' - \mathbf{x}|)) = \delta(|\mathbf{x}' - \mathbf{x}|) \tag{9}$$

Based on Eq. (9), the nonlocal constitutive relation in Eqs. (2), (3) and (4) is reduced to the differential equation by

$$L(t_{ij}) = (1 - l^2\nabla^2)\sigma_{ij} \tag{10}$$

$$L(d_i) = (1 - l^2\nabla^2)D_i \tag{11}$$

$$L(b_i) = (1 - l^2\nabla^2)B_i \tag{12}$$

where the differential operator is taken by $L = (1 - \mu^2\nabla^2)$ and μ is a nonlocal parameter.

As a result, the integro-partial differential Eqs. (6)–(8) simplifies to the following partial differential equation

$$L(t_{ij,j}) - L\left(\rho\ddot{u}_i\right) = 0 \tag{13}$$

$$L(d_{i,i}) = 0 \tag{14}$$

$$L(b_{i,i}) = 0 \tag{15}$$

By replacing Eqs. (10)–(12) into Eqs. (13)–(15), the partial differential equations can be reformulated

$$(1 - l^2\nabla^2)\sigma_{ij,j} - (1 - \mu^2\nabla^2)\left(\rho\ddot{u}_i\right) = 0 \tag{16}$$

$$(1 - l^2\nabla^2)D_{i,i} = 0 \tag{17}$$

$$(1 - l^2\nabla^2)B_{i,i} = 0 \tag{18}$$

The equations of motion for the nonlocal MEE continuum body are derived based on the principle of extended virtual work into Eqs. (16)–(18). The procedure involves by multiplication with the respective virtual fields: δu_i (virtual displacement), $\delta\Phi_i$ (virtual electric potential) and $\delta\Psi_i$ (virtual magnetic potential) by

$$\int_V (1 - l^2\nabla^2)(\delta u_i)^T\sigma_{ij,j}\mathrm{d}V - \int_V (1 - \mu^2\nabla^2)(\delta u_i)^T\rho\ddot{u}_i\mathrm{d}V + \int_V (1 - l^2\nabla^2)(\delta\Phi_i)^T D_{i,i}\mathrm{d}V + \int_V (1 - l^2\nabla^2)(\delta\Psi_i)^T B_{i,i}\mathrm{d}V = 0 \tag{19}$$

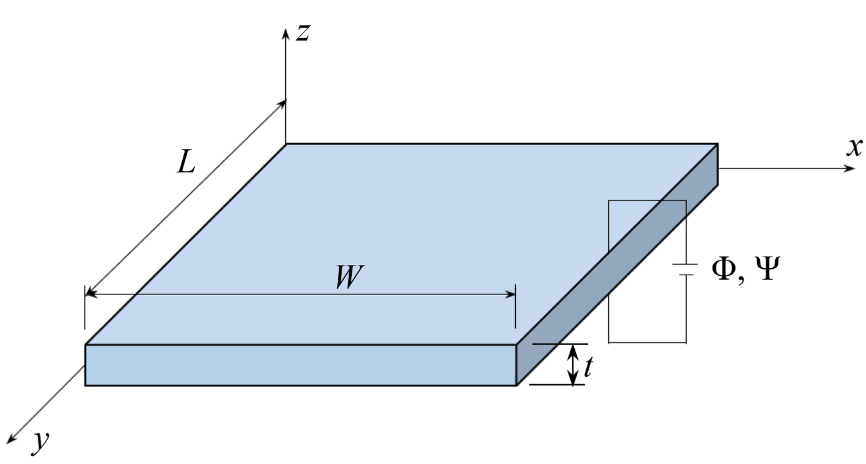

Fig. 1. Schematic diagram of the FG-MEE nanoplate.

Applying the divergence theorem (integration by parts) to the first, third and fourth terms in Eq. (19) yields respectively

$$\int_V (1-l^2\nabla^2)(\delta u_i)^T\sigma_{ij,j}dV = -\int_V (1-l^2\nabla^2)\left(\delta u_{i,j}\right)^T\sigma_{ij}dV + \int_\Gamma (1-l^2\nabla^2)(\delta u_i)^T\sigma_{ij}\overline{n}_i d\Gamma \tag{20}$$

$$\int_V (1-l^2\nabla^2)(\delta\Phi_i)^T D_{i,i}dV = -\int_V (1-l^2\nabla^2)\left(\delta\Phi_{i,i}\right)^T D_i dV + \int_\Gamma (1-l^2\nabla^2)(\delta\Phi_i)^T D_i\overline{n}_i d\Gamma \tag{21}$$

$$\int_V (1-l^2\nabla^2)(\delta\Psi_i)^T B_{i,i}dV = -\int_V (1-l^2\nabla^2)\left(\delta\Psi_{i,i}\right)^T B_i dV + \int_\Gamma (1-l^2\nabla^2)(\delta\Psi_i)^T B_i\overline{n}_i d\Gamma \tag{22}$$

where $\overline{n}$ is a normal vector.

After inserting Eqs. (20)–(22) into (19) and ignoring the traction on the Neumann boundary (Γ) in this study, the final equation can be rewritten as

$$\int_V \left(\delta\varepsilon_{ij}\right)^T\sigma_{ij}dV - l^2\int_V \left(\delta\varepsilon_{ij}\right)^T\nabla^2\sigma_{ij}dV - \int_V (\delta E_i)^T D_i dV + l^2\int_V (\delta E_i)^T\nabla^2 D_i dV - \int_V (\delta H_i)^T B_i dV + l^2\int_V (\delta H_i)^T\nabla^2 B_i dV + \int_V (1-\mu^2\nabla^2)(\delta u_i)^T\rho\ddot{u}_i dV = 0 \tag{23}$$

where $\delta u_{i,j} = \delta\varepsilon_{ij}$; $\delta\Phi_{i,i} = -\delta E_i$; $\delta\Psi_{i,i} = -\delta H_i$.

The governing equation in Eq. (23) can be expressed more compactly as

$$\delta U + \delta K = 0 \tag{24}$$

where

$$\begin{aligned}
\delta U &= \delta U_0 + \delta U_1, \delta U_0 = \int_V \left(\delta\varepsilon_{ij}\right)^T\sigma_{ij}dV - \int_V (\delta E_i)^T D_i dV - \int_V (\delta H_i)^T B_i dV \\
\delta U_1 &= -l^2\int_V \left(\delta\varepsilon_{ij}\right)^T\nabla^2\sigma_{ij}dV + l^2\int_V (\delta E_i)^T\nabla^2 D_i dV + l^2\int_V (\delta H_i)^T\nabla^2 B_i dV \\
\delta K &= \int_V (1-\mu^2\nabla^2)(\delta u_i)^T\rho\ddot{u}_i dV
\end{aligned} \tag{25}$$

in which δU is the virtual strain energy and δK is virtual kinetic energy.

2.3. HSDTs integrated to NSGT

This subsection presents the impact of different kinematic fields within the NSGT on free vibration analysis of FG-MEE nanoplates. Three representative higher-order shear deformation theories are considered: the four-variable (HSDT-4 [68]), five-variable (HSDT-5 [16]) and seven-variable (HSDT-7 [69]) models. The HSDT-5 model serves the baseline theory, while HSDT-4 and HSDT-7 are derived two variants. The selected HSDT dictates displacement fields, which is defined for an arbitrary point below.

$$\breve{\mathbf{u}}(x,y,z) = \mathbf{u}^1(x,y) + z\mathbf{u}^2(x,y) + h(z)\mathbf{u}^3(x,y) \tag{26}$$

where $\breve{\mathbf{u}} = \left\{\breve{u} \quad \breve{v} \quad \breve{w}\right\}^T$ and

$$\text{HSDT}-4\ [68]:\ \mathbf{u}^1 = \begin{Bmatrix} u \\ v \\ w^b + w^s \end{Bmatrix};\ \mathbf{u}^2 = -\begin{Bmatrix} w^b_{,x} \\ w^b_{,y} \\ 0 \end{Bmatrix};\ \mathbf{u}^3 = \begin{Bmatrix} w^s_{,x} \\ w^s_{,y} \\ 0 \end{Bmatrix};\ \text{where } u \text{ and } v \text{ are the inplane displacements; } w^b \text{ and } w^s \text{ are bending and shear transverse displacements.} \tag{27}$$

$$\text{HSDT}-5\ [16]:\ \mathbf{u}^1 = \begin{Bmatrix} u \\ v \\ w \end{Bmatrix};\ \mathbf{u}^2 = -\begin{Bmatrix} w_{,x} \\ w_{,y} \\ 0 \end{Bmatrix};\ \mathbf{u}^3 = \begin{Bmatrix} \theta_x \\ \theta_y \\ 0 \end{Bmatrix};\ \text{where } u,\ v \text{ and } w \text{ are the inplane and transverse displacements; } \theta_x \text{ and } \theta_x \text{ are two rotations.} \tag{28}$$

$$\text{HSDT}-7\ [69]:\ \mathbf{u}^1 = \begin{Bmatrix} u \\ v \\ w \end{Bmatrix};\ \mathbf{u}^2 = -\begin{Bmatrix} \beta_x \\ \beta_y \\ 0 \end{Bmatrix};\ \mathbf{u}^3 = \begin{Bmatrix} \theta_x \\ \theta_y \\ 0 \end{Bmatrix};\ \text{where } u,\ v \text{ and } w \text{ are the inplane and transverse displacements; } \beta_x \text{ and } \beta_y \text{ are two rotations; } \theta_x \text{ and } \theta_y \text{ are artificial two rotations.} \tag{29}$$

The zero shear stress condition at the plate's upper and lower surfaces is satisfied using different functions. In this study, for HSDT-5 and HSDT-7, a third-order Chebyshev polynomial, $h(z) = \cos(3 \times \cos^{-1}(z/t))$, (similar to Refs., [70,71]) is employed, whereas a different function, $h(z) = \cos(3 \times \cos^{-1}(z/t)) - z$ is used for HSDT-4.

Strain components can be written by

$$\boldsymbol{\varepsilon} = \begin{Bmatrix} \boldsymbol{\varepsilon}^b \\ \boldsymbol{\gamma} \end{Bmatrix} = \begin{Bmatrix} \{ \varepsilon_x \quad \varepsilon_y \quad \gamma_{xy} \}^{\mathrm{T}} \\ \{ \gamma_{xz} \quad \gamma_{yz} \}^{\mathrm{T}} \end{Bmatrix} \tag{30}$$

Bending and shear strain components derived from Eq. (26) are defined as

$$\text{HSDT} - 4: \ \boldsymbol{\varepsilon}^b = \boldsymbol{\varepsilon}^{b1} + z\boldsymbol{\varepsilon}^{b2} + h(z)\boldsymbol{\varepsilon}^{b3}; \ \boldsymbol{\gamma} = (1 + h'(z))\boldsymbol{\varepsilon}^s$$

$$\boldsymbol{\varepsilon}^{b1} = \begin{Bmatrix} u_{,x} \\ v_{,y} \\ u_{,y} + v_{,x} \end{Bmatrix}; \ \boldsymbol{\varepsilon}^{b2} = -\begin{Bmatrix} w^b_{,xx} \\ w^b_{,yy} \\ 2w^b_{,xy} \end{Bmatrix}; \ \boldsymbol{\varepsilon}^{b3} = \begin{Bmatrix} w^s_{,xx} \\ w^s_{,yy} \\ 2w^s_{,xy} \end{Bmatrix}; \ \boldsymbol{\varepsilon}^s = \begin{Bmatrix} w^s_{,x} \\ w^s_{,y} \end{Bmatrix} \tag{31}$$

$$\text{HSDT} - 5: \ \boldsymbol{\varepsilon}^b = \boldsymbol{\varepsilon}^{b1} + z\boldsymbol{\varepsilon}^{b2} + h(z)\boldsymbol{\varepsilon}^{b3}; \ \boldsymbol{\gamma} = h'(z)\boldsymbol{\varepsilon}^s$$

$$\boldsymbol{\varepsilon}^{b1} = \begin{Bmatrix} u_{,x} \\ v_{,y} \\ u_{,y} + v_{,x} \end{Bmatrix}; \ \boldsymbol{\varepsilon}^{b2} = -\begin{Bmatrix} w_{,xx} \\ w_{,yy} \\ 2w_{,xy} \end{Bmatrix}; \ \boldsymbol{\varepsilon}^{b3} = \begin{Bmatrix} \theta_{x,x} \\ \theta_{y,y} \\ \theta_{x,y} + \theta_{y,x} \end{Bmatrix}; \ \boldsymbol{\varepsilon}^s = \begin{Bmatrix} \theta_x \\ \theta_y \end{Bmatrix} \tag{32}$$

$$\text{HSDT} - 7: \ \boldsymbol{\varepsilon}^b = \boldsymbol{\varepsilon}^{b1} + z\boldsymbol{\varepsilon}^{b2} + h(z)\boldsymbol{\varepsilon}^{b3}; \ \boldsymbol{\gamma} = \boldsymbol{\varepsilon}^{s1} + h'(z)\boldsymbol{\varepsilon}^{s2}$$

$$\boldsymbol{\varepsilon}^{b1} = \begin{Bmatrix} u_{,x} \\ v_{,y} \\ u_{,y} + v_{,x} \end{Bmatrix}; \ \boldsymbol{\varepsilon}^{b2} = -\begin{Bmatrix} \beta_{x,x} \\ \beta_{y,y} \\ \beta_{x,y} + \beta_{y,x} \end{Bmatrix}; \ \boldsymbol{\varepsilon}^{b3} = \begin{Bmatrix} \theta_{x,x} \\ \theta_{y,y} \\ \theta_{x,y} + \theta_{y,x} \end{Bmatrix} \tag{33}$$

$$\boldsymbol{\varepsilon}^{s1} = \begin{Bmatrix} w_{,x} - \beta_x \\ w_{,y} - \beta_y \end{Bmatrix}; \ \boldsymbol{\varepsilon}^{s2} = \begin{Bmatrix} \theta_x \\ \theta_y \end{Bmatrix}$$

where $h'(z) = \frac{\mathrm{d}h(z)}{\mathrm{d}z}$.

In this study, the electric and magnetic potentials follow the formulation presented in [27].

$$\begin{aligned} \Phi(x,y,z,t) &= g(z)\varphi(x,y,t) + \frac{2z}{t}V_0 \\ \Psi(x,y,z,t) &= g(z)\psi(x,y,t) + \frac{2z}{t}\Omega_0 \end{aligned} \tag{34}$$

where the initial applied external electric voltage and magnetic potentials are expressed by V_0 and Ω_0, respectively; $g(z) = -\cos(\pi z/t)$.

The respective components for the electric field and magnetic field are defined as

$$\mathbf{E} = \begin{Bmatrix} E_x \\ E_y \\ E_z \end{Bmatrix} = -\begin{Bmatrix} \Phi_{,x} \\ \Phi_{,y} \\ \Phi_{,z} \end{Bmatrix} = -\begin{Bmatrix} g(z)\varphi_{,x} \\ g(z)\varphi_{,y} \\ g'(z)\varphi + \dfrac{2V_0}{t} \end{Bmatrix}; \ \mathbf{H} = \begin{Bmatrix} H_x \\ H_y \\ H_z \end{Bmatrix} = -\begin{Bmatrix} \Psi_{,x} \\ \Psi_{,y} \\ \Psi_{,z} \end{Bmatrix} = -\begin{Bmatrix} g(z)\psi_{,x} \\ g(z)\psi_{,y} \\ g'(z)\psi + \dfrac{2\Omega_0}{t} \end{Bmatrix} \tag{35}$$

where $g'(z) = \frac{\mathrm{d}g(z)}{\mathrm{d}z}$.

The virtual strain energy in Eq. (24) can be alternatively expressed in the following form to simplify computation

$$\begin{aligned} \delta U_0 = &\int_\Omega \delta(\hat{\varepsilon}^b)^T (\hat{\mathbf{D}}^b_{uu}\hat{\varepsilon}^b - \hat{\mathbf{D}}^b_{ue}\hat{\mathbf{E}}^b - \hat{\mathbf{D}}^b_{um}\hat{\mathbf{H}}^b)\mathrm{d}\Omega + \int_\Omega \delta(\hat{\varepsilon}^s)^T (\hat{\mathbf{D}}^s_{uu}\hat{\varepsilon}^s - \hat{\mathbf{D}}^s_{ue}\hat{\mathbf{E}}^s - \hat{\mathbf{D}}^s_{um}\hat{\mathbf{H}}^s)\mathrm{d}\Omega \\ &- \int_\Omega \delta(\hat{\mathbf{E}}^b)^T (\hat{\mathbf{D}}^b_{eu}\hat{\varepsilon}^b + \hat{\mathbf{D}}^b_{ee}\hat{\mathbf{E}}^b + \hat{\mathbf{D}}^b_{em}\hat{\mathbf{H}}^b)\mathrm{d}\Omega - \int_\Omega \delta(\hat{\mathbf{E}}^s)^T (\hat{\mathbf{D}}^s_{eu}\hat{\varepsilon}^s + \hat{\mathbf{D}}^s_{ee}\hat{\mathbf{E}}^s + \hat{\mathbf{D}}^s_{em}\hat{\mathbf{H}}^s)\mathrm{d}\Omega \\ &- \int_\Omega \delta(\hat{\mathbf{H}}^b)^T (\hat{\mathbf{D}}^b_{mu}\hat{\varepsilon}^b + \hat{\mathbf{D}}^b_{me}\hat{\mathbf{E}}^b + \hat{\mathbf{D}}^b_{mm}\hat{\mathbf{H}}^b)\mathrm{d}\Omega - \int_\Omega \delta(\hat{\mathbf{H}}^s)^T (\hat{\mathbf{D}}^s_{mu}\hat{\varepsilon}^s + \hat{\mathbf{D}}^s_{me}\hat{\mathbf{E}}^s + \hat{\mathbf{D}}^s_{mm}\hat{\mathbf{H}}^s)\mathrm{d}\Omega \end{aligned} \tag{36}$$

$$\begin{aligned} \delta U_1 = &-l^2 \int_\Omega \delta(\hat{\varepsilon}^b)^T \nabla^2 (\hat{\mathbf{D}}^b_{uu}\hat{\varepsilon}^b - \hat{\mathbf{D}}^b_{ue}\hat{\mathbf{E}}^b - \hat{\mathbf{D}}^b_{um}\hat{\mathbf{H}}^b)\mathrm{d}\Omega - l^2 \int_\Omega \delta(\hat{\varepsilon}^s)^T \nabla^2 (\hat{\mathbf{D}}^s_{uu}\hat{\varepsilon}^s - \hat{\mathbf{D}}^s_{ue}\hat{\mathbf{E}}^s - \hat{\mathbf{D}}^s_{um}\hat{\mathbf{H}}^s)\mathrm{d}\Omega \\ &+ l^2 \int_\Omega \delta(\hat{\mathbf{E}}^b)^T \nabla^2 (\hat{\mathbf{D}}^b_{eu}\hat{\varepsilon}^b + \hat{\mathbf{D}}^b_{ee}\hat{\mathbf{E}}^b + \hat{\mathbf{D}}^b_{em}\hat{\mathbf{H}}^b)\mathrm{d}\Omega + l^2 \int_\Omega \delta(\hat{\mathbf{E}}^s)^T \nabla^2 (\hat{\mathbf{D}}^s_{eu}\hat{\varepsilon}^s + \hat{\mathbf{D}}^s_{ee}\hat{\mathbf{E}}^s + \hat{\mathbf{D}}^s_{em}\hat{\mathbf{H}}^s)\mathrm{d}\Omega \\ &+ l^2 \int_\Omega \delta(\hat{\mathbf{H}}^b)^T \nabla^2 (\hat{\mathbf{D}}^b_{mu}\hat{\varepsilon}^b + \hat{\mathbf{D}}^b_{me}\hat{\mathbf{E}}^b + \hat{\mathbf{D}}^b_{mm}\hat{\mathbf{H}}^b)\mathrm{d}\Omega + l^2 \int_\Omega \delta(\hat{\mathbf{H}}^s)^T \nabla^2 (\hat{\mathbf{D}}^s_{mu}\hat{\varepsilon}^s + \hat{\mathbf{D}}^s_{me}\hat{\mathbf{E}}^s + \hat{\mathbf{D}}^s_{mm}\hat{\mathbf{H}}^s)\mathrm{d}\Omega \end{aligned}$$

where Ω is an area of the middle-surface of plates and

$$\text{HSDT}-4:\ \hat{\varepsilon}^b=\begin{Bmatrix}\boldsymbol{\varepsilon}^{b1}\\ \boldsymbol{\varepsilon}^{b2}\\ \boldsymbol{\varepsilon}^{b3}\end{Bmatrix};\ \hat{\varepsilon}^s=\boldsymbol{\varepsilon}^s;\ \hat{\mathbf{E}}^b=-\begin{Bmatrix}0\\0\\\varphi\end{Bmatrix};\ \hat{\mathbf{E}}^s=-\begin{Bmatrix}\varphi_{,x}\\ \varphi_{,y}\end{Bmatrix};\ \hat{\mathbf{H}}^b=-\begin{Bmatrix}0\\0\\\psi\end{Bmatrix}$$

$$\hat{\mathbf{H}}^s=-\begin{Bmatrix}\psi_{,x}\\ \psi_{,y}\end{Bmatrix};\ \hat{\mathbf{D}}^b_{uu}=\begin{bmatrix}\mathbf{A}^b & \mathbf{B}^b & \mathbf{E}^b\\ \mathbf{B}^b & \mathbf{D}^b & \mathbf{F}^b\\ \mathbf{E}^b & \mathbf{F}^b & \mathbf{H}^b\end{bmatrix};\ \hat{\mathbf{D}}^s_{uu}=\mathbf{D}^s;\quad \mathbf{D}^s=\int_{-h/2}^{h/2}(1+h'(z))^2\mathbf{C}_{uus}\mathrm{d}z$$

$$\begin{aligned}
\left(\mathbf{A}^b,\mathbf{B}^b,\mathbf{D}^b,\mathbf{E}^b,\mathbf{F}^b,\mathbf{H}^b\right)&=\int_{-h/2}^{h/2}\left(1,z,z^2,h(z),zh(z),h^2(z)\right)\mathbf{C}_{uub}\mathrm{d}z\\
\hat{\mathbf{D}}^b_{ue}=\left\{\hat{\mathbf{C}}^1_{ueb}\quad \hat{\mathbf{C}}^2_{ueb}\quad \hat{\mathbf{C}}^3_{ueb}\right\}^T;&\ \left(\hat{\mathbf{C}}^1_{ueb},\hat{\mathbf{C}}^2_{ueb},\hat{\mathbf{C}}^3_{ueb}\right)=\int_{-h/2}^{h/2}\mathbf{C}_{ueb}(1,z,h(z))g'(z)\mathrm{d}z\\
\hat{\mathbf{D}}^b_{um}=\left\{\hat{\mathbf{C}}^1_{umb}\quad \hat{\mathbf{C}}^2_{umb}\quad \hat{\mathbf{C}}^3_{umb}\right\}^T;&\ \left(\hat{\mathbf{C}}^1_{umb},\hat{\mathbf{C}}^2_{umb},\hat{\mathbf{C}}^3_{umb}\right)=\int_{-h/2}^{h/2}\mathbf{C}_{umb}(1,z,h(z))g'(z)\mathrm{d}z\\
\hat{\mathbf{D}}^s_{ue}=\hat{\mathbf{C}}_{ues};\ \hat{\mathbf{C}}_{ues}=\int_{-h/2}^{h/2}\mathbf{C}_{ues}(1+h'(z))g(z)\mathrm{d}z,&\ \hat{\mathbf{D}}^s_{um}=\hat{\mathbf{C}}_{ums};\ \hat{\mathbf{C}}_{ums}=\int_{-h/2}^{h/2}\mathbf{C}_{ums}(1+h'(z))g(z)\mathrm{d}z\\
\hat{\mathbf{D}}^b_{ee}=\int_{-h/2}^{h/2}\mathbf{C}_{eeb}g'^2(z)dz;\ \hat{\mathbf{D}}^s_{ee}=\int_{-h/2}^{h/2}&\mathbf{C}_{ees}g^2(z)\mathrm{d}z;\ \hat{\mathbf{D}}^b_{em}=\int_{-h/2}^{h/2}\mathbf{C}_{emb}g'^2(z)dz\\
\hat{\mathbf{D}}^s_{em}=\int_{-h/2}^{h/2}\mathbf{C}_{ems}g^2(z)\mathrm{d}z;\ \hat{\mathbf{D}}^b_{mm}=\int_{-h/2}^{h/2}&\mathbf{C}_{mmb}g'^2(z)dz;\ \hat{\mathbf{D}}^s_{mm}=\int_{-h/2}^{h/2}\mathbf{C}_{mms}g^2(z)\mathrm{d}z\\
\hat{\mathbf{D}}^b_{eu}=\left(\hat{\mathbf{D}}^b_{ue}\right)^T;\ \hat{\mathbf{D}}^s_{eu}=\left(\hat{\mathbf{D}}^s_{ue}\right)^T;\ \hat{\mathbf{D}}^b_{mu}=\left(\hat{\mathbf{D}}^b_{um}\right)^T;&\ \hat{\mathbf{D}}^s_{mu}=\left(\hat{\mathbf{D}}^s_{um}\right)^T;\ \hat{\mathbf{D}}^b_{me}=\left(\hat{\mathbf{D}}^b_{em}\right)^T;\ \hat{\mathbf{D}}^s_{me}=\left(\hat{\mathbf{D}}^s_{em}\right)^T
\end{aligned}\tag{37}$$

$$\begin{aligned}
\text{HSDT}-5:\ \hat{\boldsymbol{\varepsilon}}^b=\begin{Bmatrix}\boldsymbol{\varepsilon}^{b1}\\ \boldsymbol{\varepsilon}^{b2}\\ \boldsymbol{\varepsilon}^{b3}\end{Bmatrix},\hat{\boldsymbol{\varepsilon}}^s=\boldsymbol{\varepsilon}^s,&\ \hat{\mathbf{E}}^b=-\begin{Bmatrix}0\\0\\\varphi\end{Bmatrix},\hat{\mathbf{E}}^s=-\begin{Bmatrix}\varphi_{,x}\\ \varphi_{,y}\end{Bmatrix},\hat{\mathbf{H}}^b=-\begin{Bmatrix}0\\0\\\psi\end{Bmatrix}\\
\hat{\mathbf{H}}^s=-\begin{Bmatrix}\psi_{,x}\\ \psi_{,y}\end{Bmatrix},\hat{\mathbf{D}}^b_{uu}=&\begin{bmatrix}\mathbf{A}^b & \mathbf{B}^b & \mathbf{E}^b\\ \mathbf{B}^b & \mathbf{D}^b & \mathbf{F}^b\\ \mathbf{E}^b & \mathbf{F}^b & \mathbf{H}^b\end{bmatrix},\hat{\mathbf{D}}^s_{uu}=\mathbf{D}^s,\ \mathbf{D}^s=\int_{-h/2}^{h/2}h'^2(z)\mathbf{C}_{uus}\mathrm{d}z\\
\left(\mathbf{A}^b,\mathbf{B}^b,\mathbf{D}^b,\mathbf{E}^b,\mathbf{F}^b,\mathbf{H}^b\right)&=\int_{-h/2}^{h/2}\left(1,z,z^2,h(z),zh(z),h^2(z)\right)\mathbf{C}_{uub}\mathrm{d}z\\
\hat{\mathbf{D}}^b_{ue}=\left\{\hat{\mathbf{C}}^1_{ueb}\quad \hat{\mathbf{C}}^2_{ueb}\quad \hat{\mathbf{C}}^3_{ueb}\right\}^T;&\ \left(\hat{\mathbf{C}}^1_{ueb},\hat{\mathbf{C}}^2_{ueb},\hat{\mathbf{C}}^3_{ueb}\right)=\int_{-h/2}^{h/2}\mathbf{C}_{ueb}(1,z,h(z))g'(z)\mathrm{d}z\\
\hat{\mathbf{D}}^b_{um}=\left\{\hat{\mathbf{C}}^1_{umb}\quad \hat{\mathbf{C}}^2_{umb}\quad \hat{\mathbf{C}}^3_{umb}\right\}^T;&\ \left(\hat{\mathbf{C}}^1_{umb},\hat{\mathbf{C}}^2_{umb},\hat{\mathbf{C}}^3_{umb}\right)=\int_{-h/2}^{h/2}\mathbf{C}_{umb}(1,z,h(z))g'(z)\mathrm{d}z\\
\hat{\mathbf{D}}^s_{ue}=\hat{\mathbf{C}}_{ues};\ \hat{\mathbf{C}}_{ues}=\int_{-h/2}^{h/2}\mathbf{C}_{ues}h'(z)g(z)\mathrm{d}z;&\ \hat{\mathbf{D}}^s_{um}=\hat{\mathbf{C}}_{ums};\ \hat{\mathbf{C}}_{ums}=\int_{-h/2}^{h/2}\mathbf{C}_{ums}h'(z)g(z)\mathrm{d}z\\
\hat{\mathbf{D}}^b_{ee}=\int_{-h/2}^{h/2}\mathbf{C}_{eeb}g'^2(z)dz;\ \hat{\mathbf{D}}^s_{ee}=\int_{-h/2}^{h/2}&\mathbf{C}_{ees}g^2(z)\mathrm{d}z;\ \hat{\mathbf{D}}^b_{em}=\int_{-h/2}^{h/2}\mathbf{C}_{emb}g'^2(z)dz\\
\hat{\mathbf{D}}^s_{em}=\int_{-h/2}^{h/2}\mathbf{C}_{ems}g^2(z)\mathrm{d}z;\hat{\mathbf{D}}^b_{mm}=\int_{-h/2}^{h/2}&\mathbf{C}_{mmb}g'^2(z)dz;\ \hat{\mathbf{D}}^s_{mm}=\int_{-h/2}^{h/2}\mathbf{C}_{mms}g^2(z)\mathrm{d}z\\
\hat{\mathbf{D}}^b_{eu}=\left(\hat{\mathbf{D}}^b_{ue}\right)^T;\ \hat{\mathbf{D}}^s_{eu}=\left(\hat{\mathbf{D}}^s_{ue}\right)^T;\ \hat{\mathbf{D}}^b_{mu}=\left(\hat{\mathbf{D}}^b_{um}\right)^T;&\ \hat{\mathbf{D}}^s_{mu}=\left(\hat{\mathbf{D}}^s_{um}\right)^T;\ \hat{\mathbf{D}}^b_{me}=\left(\hat{\mathbf{D}}^b_{em}\right)^T;\ \hat{\mathbf{D}}^s_{me}=\left(\hat{\mathbf{D}}^s_{em}\right)^T
\end{aligned}\tag{38}$$

$$
\begin{aligned}
&\mathrm{HSDT}-7:\ \widehat{\boldsymbol{\varepsilon}}^{b}=\begin{Bmatrix}\boldsymbol{\varepsilon}^{b1}\\ \boldsymbol{\varepsilon}^{b2}\\ \boldsymbol{\varepsilon}^{b3}\end{Bmatrix};\ \widehat{\boldsymbol{\varepsilon}}^{s}=\begin{Bmatrix}\boldsymbol{\varepsilon}^{s1}\\ \boldsymbol{\varepsilon}^{s2}\end{Bmatrix};\ \widehat{\mathbf{E}}^{b}=-\begin{Bmatrix}0\\0\\ \varphi\end{Bmatrix};\widehat{\mathbf{E}}^{s}=-\begin{Bmatrix}\varphi_{,x}\\ \varphi_{,y}\end{Bmatrix};\widehat{\mathbf{H}}^{b}=-\begin{Bmatrix}0\\0\\ \psi\end{Bmatrix}\\
&\widehat{\mathbf{H}}^{s}=-\begin{Bmatrix}\psi_{,x}\\ \psi_{,y}\end{Bmatrix};\ \widehat{\mathbf{D}}^{b}_{uu}=\begin{bmatrix}\mathbf{A}^b & \mathbf{B}^b & \mathbf{E}^b\\ \mathbf{B}^b & \mathbf{D}^b & \mathbf{F}^b\\ \mathbf{E}^b & \mathbf{F}^b & \mathbf{H}^b\end{bmatrix};\ \widehat{\mathbf{D}}^{s}_{uu}=\begin{bmatrix}\mathbf{A}^s & \mathbf{B}^s\\ \mathbf{B}^s & \mathbf{D}^s\end{bmatrix}\\
&\left(\mathbf{A}^b,\mathbf{B}^b,\mathbf{D}^b,\mathbf{E}^b,\mathbf{F}^b,\mathbf{H}^b\right)=\int_{-h/2}^{h/2}\left(1,z,z^2,h(z),zh(z),h^2(z)\right)\mathbf{C}_{uub}\mathrm{d}z\\
&\left(\mathbf{A}^s,\mathbf{B}^s,\mathbf{D}^s\right)=\int_{-h/2}^{h/2}\left(1,h'(z),h'^2(z)\right)\mathbf{C}_{uus}\mathrm{d}z\\
&\widehat{\mathbf{D}}^{b}_{ue}=\left\{\widehat{\mathbf{C}}^{1}_{ueb}\quad \widehat{\mathbf{C}}^{2}_{ueb}\quad \widehat{\mathbf{C}}^{3}_{ueb}\right\}^T;\ \left(\widehat{\mathbf{C}}^{1}_{ueb},\widehat{\mathbf{C}}^{2}_{ueb},\widehat{\mathbf{C}}^{3}_{ueb}\right)=\int_{-h/2}^{h/2}\mathbf{C}_{ueb}(1,z,h(z))g'(z)\mathrm{d}z\\
&\widehat{\mathbf{D}}^{b}_{um}=\left\{\widehat{\mathbf{C}}^{1}_{umb}\quad \widehat{\mathbf{C}}^{2}_{umb}\quad \widehat{\mathbf{C}}^{3}_{umb}\right\}^T;\ \left(\widehat{\mathbf{C}}^{1}_{umb},\widehat{\mathbf{C}}^{2}_{umb},\widehat{\mathbf{C}}^{3}_{umb}\right)=\int_{-h/2}^{h/2}\mathbf{C}_{umb}(1,z,h(z))g'(z)\mathrm{d}z\\
&\widehat{\mathbf{D}}^{s}_{ue}=\left\{\widehat{\mathbf{C}}^{1}_{ues}\quad \widehat{\mathbf{C}}^{2}_{ues}\right\}^T;\ \left(\widehat{\mathbf{C}}^{1}_{ues},\widehat{\mathbf{C}}^{2}_{ues}\right)=\int_{-h/2}^{h/2}\mathbf{C}_{ues}(1,h'(z))g(z)\mathrm{d}z\\
&\widehat{\mathbf{D}}^{s}_{um}=\left\{\widehat{\mathbf{C}}^{1}_{ums}\quad \widehat{\mathbf{C}}^{2}_{ums}\right\}^T;\ \left(\widehat{\mathbf{C}}^{1}_{ums},\widehat{\mathbf{C}}^{2}_{ums}\right)=\int_{-h/2}^{h/2}\mathbf{C}_{ums}(1,h'(z))g(z)\mathrm{d}z\\
&\widehat{\mathbf{D}}^{b}_{ee}=\int_{-h/2}^{h/2}\mathbf{C}_{eeb}g'^2(z)dz;\ \widehat{\mathbf{D}}^{s}_{ee}=\int_{-h/2}^{h/2}\mathbf{C}_{ees}g^2(z)\mathrm{d}z;\ \widehat{\mathbf{D}}^{b}_{em}=\int_{-h/2}^{h/2}\mathbf{C}_{emb}g'^2(z)dz\\
&\widehat{\mathbf{D}}^{s}_{em}=\int_{-h/2}^{h/2}\mathbf{C}_{ems}g^2(z)\mathrm{d}z;\ \widehat{\mathbf{D}}^{b}_{mm}=\int_{-h/2}^{h/2}\mathbf{C}_{mmb}g'^2(z)dz;\ \widehat{\mathbf{D}}^{s}_{mm}=\int_{-h/2}^{h/2}\mathbf{C}_{mms}g^2(z)\mathrm{d}z\\
&\widehat{\mathbf{D}}^{b}_{eu}=\left(\widehat{\mathbf{D}}^{b}_{ue}\right)^T;\ \widehat{\mathbf{D}}^{s}_{eu}=\left(\widehat{\mathbf{D}}^{s}_{ue}\right)^T;\ \widehat{\mathbf{D}}^{b}_{mu}=\left(\widehat{\mathbf{D}}^{b}_{um}\right)^T;\ \widehat{\mathbf{D}}^{s}_{mu}=\left(\widehat{\mathbf{D}}^{s}_{um}\right)^T\\
&\mathbf{D}^{b}_{me}=\left(\widehat{\mathbf{D}}^{b}_{em}\right)^T;\ \widehat{\mathbf{D}}^{s}_{me}=\left(\widehat{\mathbf{D}}^{s}_{em}\right)^T
\end{aligned}
\tag{39}
$$

in which

$$
\begin{aligned}
&\mathbf{C}_{uub}=\begin{bmatrix}\widehat{c}_{11}&\widehat{c}_{12}&0\\ \widehat{c}_{21}&\widehat{c}_{22}&0\\0&0&\widehat{c}_{66}\end{bmatrix};\ \mathbf{C}_{ueb}=\begin{bmatrix}0&0&\widehat{e}_{31}\\0&0&\widehat{e}_{32}\\0&0&0\end{bmatrix};\ \mathbf{C}_{umb}=\begin{bmatrix}0&0&\widehat{q}_{31}\\0&0&\widehat{q}_{32}\\0&0&0\end{bmatrix};\ \mathbf{C}_{eeb}=\begin{bmatrix}0&0&0\\0&0&0\\0&0&\widehat{k}_{33}\end{bmatrix}\\
&\mathbf{C}_{uus}=\begin{bmatrix}\widehat{c}_{55}&0\\0&\widehat{c}_{44}\end{bmatrix};\ \mathbf{C}_{ues}=\begin{bmatrix}\widehat{e}_{15}&0\\0&\widehat{e}_{24}\end{bmatrix};\ \mathbf{C}_{ums}=\begin{bmatrix}\widehat{q}_{15}&0\\0&\widehat{q}_{24}\end{bmatrix};\ \mathbf{C}_{ees}=\begin{bmatrix}\widehat{k}_{11}&0\\0&\widehat{k}_{22}\end{bmatrix}\\
&\mathbf{C}_{emb}=\begin{bmatrix}0&0&0\\0&0&0\\0&0&\widehat{d}_{33}\end{bmatrix};\ \mathbf{C}_{mmb}=\begin{bmatrix}0&0&0\\0&0&0\\0&0&\widehat{\mu}_{33}\end{bmatrix};\ \mathbf{C}_{ems}=\begin{bmatrix}\widehat{d}_{11}&0\\0&\widehat{d}_{22}\end{bmatrix};\ \mathbf{C}_{mms}=\begin{bmatrix}\widehat{\mu}_{11}&0\\0&\widehat{\mu}_{22}\end{bmatrix}
\end{aligned}
\tag{40}
$$

For the plane stress case, the reduced material properties from Eq. (40) are calculated [27]

$$
\begin{aligned}
&\widehat{c}_{11}=c_{11}-\frac{c_{13}^2}{c_{33}};\widehat{c}_{12}=c_{12}-\frac{c_{13}^2}{c_{33}};\widehat{c}_{66}=c_{66};\widehat{c}_{55}=c_{55};\widehat{c}_{44}=c_{44}\\
&\widehat{e}_{31}=e_{31}-\frac{e_{33}c_{13}}{c_{33}};\widehat{e}_{15}=e_{15};\widehat{q}_{31}=q_{31}-\frac{q_{33}c_{13}}{c_{33}};\widehat{q}_{15}=q_{15}\\
&\widehat{k}_{33}=k_{33}+\frac{e_{33}^2}{c_{33}};\widehat{k}_{11}=k_{11};\widehat{d}_{33}=d_{33}+\frac{q_{33}e_{33}}{c_{33}};\widehat{d}_{11}=d_{11};\widehat{\mu}_{33}=\mu_{33}+\frac{q_{33}^2}{c_{33}};\widehat{\mu}_{11}=\mu_{11}
\end{aligned}
\tag{41}
$$

The effective material properties of FG-MEE nanoplates are determined using the power-law scheme, as expressed in Eq. (1).

The virtual kinetic energy from Eq. (24) is likewise defined as

$$
\delta K=\int_{\Omega}\left(1-\mu\nabla^2\right)\delta\widehat{\mathbf{u}}^T\widehat{\mathbf{I}}\ddot{\widehat{\mathbf{u}}}\mathrm{d}\Omega \tag{42}
$$

where

$$
\begin{aligned}
\widehat{\mathbf{u}}=\begin{Bmatrix}\mathbf{u}^1\\ \mathbf{u}^2\\ \mathbf{u}^3\end{Bmatrix};\ \widehat{\mathbf{I}}=\begin{bmatrix}\mathbf{I}_1&\mathbf{I}_2&\mathbf{I}_4\\ \mathbf{I}_2&\mathbf{I}_3&\mathbf{I}_5\\ \mathbf{I}_4&\mathbf{I}_5&\mathbf{I}_6\end{bmatrix};\ &(\mathbf{I}_1,\mathbf{I}_2,\mathbf{I}_3,\mathbf{I}_4,\mathbf{I}_5,\mathbf{I}_6)\\
&=\int_{-h/2}^{h/2}\rho\left(1,z,z^2,h(z),zh(z),h^2(z)\right)\mathbf{I}_{3\times3}\mathrm{d}z
\end{aligned}
\tag{43}
$$

where $\mathbf{I}_{3\times3}$ is the 3 × 3 identity matrix, while ρ is also computed by Eq. (1).

Furthermore, by accounting for the pre-buckling forces (mechanical, electrical and magnetic), the potential energy variation resulting from these in-plane loads is

$$\text{HSDT}-4:\ \delta W=-\int_{\Omega}(1-\mu^2\nabla^2)\delta\begin{Bmatrix} w^b_{,x}+w^s_{,x} \\ w^b_{,y}+w^s_{,y}\end{Bmatrix}^{\mathrm{T}}\begin{bmatrix} N^0_x & 0 \\ 0 & N^0_y\end{bmatrix}\begin{Bmatrix} w^b_{,x}+w^s_{,x} \\ w^b_{,y}+w^s_{,y}\end{Bmatrix}d\Omega \tag{44}$$

$$\text{HSDT}-5\ \text{and HSDT}-7:\ \delta W=-\int_{\Omega}(1-\mu^2\nabla^2)\delta\begin{Bmatrix} w_{,x} \\ w_{,y}\end{Bmatrix}^{\mathrm{T}}\begin{bmatrix} N^0_x & 0 \\ 0 & N^0_y\end{bmatrix}\begin{Bmatrix} w_{,x} \\ w_{,y}\end{Bmatrix}d\Omega \tag{45}$$

The potential energy variation can be rewritten by a different form as follows

$$\delta W=-\int_{\Omega}(1-\mu^2\nabla^2)\delta(\mathbf{B}^g)^{\mathrm{T}}\begin{bmatrix} N^{mech}_x+N^{elec}_x+N^{mag}_x & 0 \\ 0 & N^{mech}_y+N^{elec}_y+N^{mag}_y\end{bmatrix}\mathbf{B}^g d\Omega \tag{46}$$

here N^{mech}_x and N^{mech}_y are the in-plane mechanical loads and the other components are defined as $N^{elec}_x = N^{elec}_y = 2\bar{e}_{31}V_0$; $N^{mag}_x = N^{mag}_y = 2\bar{q}_{31}\Omega_0$ [29,42].

For free vibration, the governing equations derived from Eq. (24) are as follows

$$\delta U+\delta K-\delta W=0 \tag{47}$$

2.4. NURBS basis function for NSGT

Isogeometric analysis (IGA) introduced by Hughes et al. [47] is a well-established computational framework. To maintain conciseness, the fundamental mathematical formulations of the IGA and Non-Uniform Rational B-Splines (NURBS) are not repeated here and can be found in Ref. [47]. The IGA relies on NURBS basis functions with inherent high-order continuity, making it particularly well suited for analyzing MEE nanoplates within the NSGT. Specifically, a NURBS basis function of degree p ensures up to C^{p-1} across internal knot spans. Utilizing these basis functions, the extended displacement field can be approximated as

$$\mathbf{u}^h(x,y)=\sum_{I=1}^{m\times n}R_I(x,y)\mathbf{I}_R\mathbf{d}_I \tag{48}$$

where R_I is NURBS basis functions and

HSDT-4: $\mathbf{d}_I=\{u_I\ \ v_I\ \ w^b_I\ \ w^b_I\ \ \varphi_I\ \ \psi_I\}^T$; $\mathbf{I}_R$ is the 6 × 6 identity matrix

HSDT-5: $\mathbf{d}_I=\{u_I\ \ v_I\ \ w_I\ \ \theta_{xI}\ \ \theta_{yI}\ \ \varphi_I\ \ \psi_I\}^T$; $\mathbf{I}_R$ is the 7 × 7 identity matrix

HSDT-7: $\mathbf{d}_I=\{u_I\ \ v_I\ \ w_I\ \ \theta_{xI}\ \ \theta_{yI}\ \ \beta_{xI}\ \ \beta_{yI}\ \ \varphi_I\ \ \psi_I\}^T$; $\mathbf{I}_R$ is the 9 × 9 identity matrix

By substituting Eq. (48) into Eqs. (31)–(33), the equation becomes

HSDT-4 and HSDT-5: $\widehat{\boldsymbol{\varepsilon}}^b=\{\boldsymbol{\varepsilon}^{b1}\ \ \boldsymbol{\varepsilon}^{b2}\ \ \boldsymbol{\varepsilon}^{b3}\}^T=\sum_{I=1}^{m\times n}\{\mathbf{B}^{b1}_I\ \ \mathbf{B}^{b2}_I\ \ \mathbf{B}^{b3}_I\}^T\mathbf{d}_I=\sum_{I=1}^{m\times n}\widehat{\mathbf{B}}^b_I\mathbf{d}_I$

Table 1
Material properties [72].

Properties	$BaTiO_3$	$CoFe_2O_4$
$c_{11}=c_{22}$ (GPa)	166	286
c_{33}	162	269.5
$c_{13}=c_{23}$	78	170.5
c_{12}	77	173
c_{55}	43	45.3
c_{66}	44.5	56.5
e_{31}(C/m^2)	−4.4	0
e_{33}	18.6	0
e_{15}	11.6	0
q_{31} (N/Am)	0	580.3
q_{33}	0	699.7
q_{15}	0	550
k_{11} (10^{-9} C^2/m^{2}N^1)	11.2	0.08
k_{33}	12.6	0.093
μ_{11}(10^{-6} Ns^2/C^2)	5	−590
μ_{33}	10	157
$d_{11}=d_{22}=d_{33}$ (10^{-12} Ns/VC)	0	0
ρ (kg/m^3)	5800	5300

$$\widehat{\boldsymbol{\varepsilon}}^s=\boldsymbol{\varepsilon}^s=\sum_{I=1}^{m\times n}\mathbf{B}^s_I\mathbf{d}_I=\sum_{I=1}^{m\times n}\widehat{\mathbf{B}}^s_I\mathbf{d}_I \tag{49}$$

$$\begin{gathered}\text{HSDT}-7:\ \widehat{\boldsymbol{\varepsilon}}^b=\{\boldsymbol{\varepsilon}^{b1}\ \ \boldsymbol{\varepsilon}^{b2}\ \ \boldsymbol{\varepsilon}^{b3}\}^T=\sum_{I=1}^{m\times n}\{\mathbf{B}^{b1}_I\ \ \mathbf{B}^{b2}_I\ \ \mathbf{B}^{b3}_I\}^T\mathbf{d}_I=\sum_{I=1}^{m\times n}\widehat{\mathbf{B}}^b_I\mathbf{d}_I \\ \widehat{\boldsymbol{\varepsilon}}^s=\{\boldsymbol{\varepsilon}^{s1}\ \ \boldsymbol{\varepsilon}^{s2}\}^T=\sum_{I=1}^{m\times n}\{\mathbf{B}^{s1}_I\ \ \mathbf{B}^{s2}_I\}^T\mathbf{d}_I=\sum_{I=1}^{m\times n}\widehat{\mathbf{B}}^s_I\mathbf{d}_I\end{gathered} \tag{50}$$

where

$$\begin{gathered}\text{HSDT}-4:\ \mathbf{B}^{b1}_I=\begin{bmatrix} R_{I,x} & 0 & 0 & 0 & 0 & 0 \\ 0 & R_{I,y} & 0 & 0 & 0 & 0 \\ R_{I,y} & R_{I,x} & 0 & 0 & 0 & 0\end{bmatrix};\ \mathbf{B}^{b2}_I=-\begin{bmatrix} 0 & 0 & R_{I,xx} & 0 & 0 & 0 \\ 0 & 0 & R_{I,yy} & 0 & 0 & 0 \\ 0 & 0 & 2R_{I,xy} & 0 & 0 & 0\end{bmatrix} \\ \mathbf{B}^{b3}_I=\begin{bmatrix} 0 & 0 & 0 & R_{I,xx} & 0 & 0 \\ 0 & 0 & 0 & R_{I,yy} & 0 & 0 \\ 0 & 0 & 0 & 2R_{I,xy} & 0 & 0\end{bmatrix};\ \mathbf{B}^s_I=\begin{bmatrix} 0 & 0 & 0 & R_{I,x} & 0 & 0 \\ 0 & 0 & 0 & R_{I,y} & 0 & 0\end{bmatrix}\end{gathered} \tag{51}$$

$$\begin{gathered}\text{HSDT}-5:\ \mathbf{B}^{b1}_I=\begin{bmatrix} R_{I,x} & 0 & 0 & 0 & 0 & 0 & 0 \\ 0 & R_{I,y} & 0 & 0 & 0 & 0 & 0 \\ R_{I,y} & R_{I,x} & 0 & 0 & 0 & 0 & 0\end{bmatrix};\ \mathbf{B}^{b2}_I=-\begin{bmatrix} 0 & 0 & R_{I,xx} & 0 & 0 & 0 & 0 \\ 0 & 0 & R_{I,yy} & 0 & 0 & 0 & 0 \\ 0 & 0 & 2R_{I,xy} & 0 & 0 & 0 & 0\end{bmatrix} \\ \mathbf{B}^{b3}_I=\begin{bmatrix} 0 & 0 & 0 & R_{I,x} & 0 & 0 & 0 \\ 0 & 0 & 0 & 0 & R_{I,y} & 0 & 0 \\ 0 & 0 & 0 & R_{I,y} & R_{I,x} & 0 & 0\end{bmatrix};\ \mathbf{B}^s_I=\begin{bmatrix} 0 & 0 & 0 & R_I & 0 & 0 & 0 \\ 0 & 0 & 0 & 0 & R_I & 0 & 0\end{bmatrix}\end{gathered} \tag{52}$$

$$\begin{gathered}\text{HSDT}-7:\ \mathbf{B}^{b1}_I=\begin{bmatrix} R_{I,x} & 0 & 0 & 0 & 0 & 0 & 0 & 0 & 0 \\ 0 & R_{I,y} & 0 & 0 & 0 & 0 & 0 & 0 & 0 \\ R_{I,y} & R_{I,x} & 0 & 0 & 0 & 0 & 0 & 0 & 0\end{bmatrix} \\ \mathbf{B}^{b2}_I=-\begin{bmatrix} 0 & 0 & 0 & 0 & 0 & R_{I,x} & 0 & 0 & 0 \\ 0 & 0 & 0 & 0 & 0 & 0 & R_{I,y} & 0 & 0 \\ 0 & 0 & 0 & 0 & 0 & R_{I,y} & R_{I,x} & 0 & 0\end{bmatrix} \\ \mathbf{B}^{b3}_I=\begin{Bmatrix} 0 & 0 & 0 & R_{I,x} & 0 & 0 & 0 & 0 & 0 \\ 0 & 0 & 0 & 0 & R_{I,y} & 0 & 0 & 0 & 0 \\ 0 & 0 & 0 & R_{I,y} & R_{I,x} & 0 & 0 & 0 & 0\end{Bmatrix} \\ \mathbf{B}^{s1}_I=\begin{bmatrix} 0 & 0 & R_{I,x} & 0 & 0 & -R_I & 0 & 0 & 0 \\ 0 & 0 & R_{I,y} & 0 & 0 & 0 & -R_I & 0 & 0\end{bmatrix} \\ \mathbf{B}^{s2}_I=\begin{bmatrix} 0 & 0 & 0 & R_I & 0 & 0 & 0 & 0 & 0 \\ 0 & 0 & 0 & 0 & R_I & 0 & 0 & 0 & 0\end{bmatrix}\end{gathered} \tag{53}$$

Table 2
The boundary conditions.

HSDTs	Type BCs	Conditions
HSDT-4	Simply supported	$\begin{cases} (v, w^b, w^s, \varphi, \psi) = 0, & \text{along}\, x = 0, a \\ (u, w^b, w^s, \varphi, \psi) = 0, & \text{along}\, y = 0, b \end{cases}$
	Fully clamped	$\begin{cases} (u, v, w^b, w^s, \varphi, \psi) = 0, & \text{along}\, x = 0, a\, \text{and}\, y = 0, b \\ \left(\dfrac{\partial w^b}{\partial n}, \dfrac{\partial w^s}{\partial n}\right) = 0, & \text{along}\, x = 0, a\, \text{and}\, y = 0, b \end{cases}$
HSDT-5	Simply supported	$\begin{cases} (v, w, \beta_y, \varphi, \psi) = 0, & \text{along}\, x = 0, a \\ (u, w, \beta_x, \varphi, \psi) = 0, & \text{along}\, y = 0, b \end{cases}$
	Fully clamped	$\begin{cases} (u, v, w, \beta_x, \beta_y, \varphi, \psi) = 0, & \text{along}\, x = 0, a\, \text{and}\, y = 0, b \\ \left(\dfrac{\partial w}{\partial n}\right) = 0, & \text{along}\, x = 0, a\, \text{and}\, y = 0, b \end{cases}$
HSDT-7	Simply supported	$\begin{cases} (v, w, \theta_y, \beta_y, \varphi, \psi) = 0, & \text{along}\, x = 0, a \\ (u, w, \theta_x, \beta_x, \varphi, \psi) = 0, & \text{along}\, y = 0, b \end{cases}$
	Fully clamped	$(u, v, w, \theta_x, \theta_y, \beta_x, \beta_y, \varphi, \psi)\, \text{along}\, x = 0, a\, \text{and}\, y = 0, b$

Substituting Eqs. (51)–(53) into Eq. (36) leads to weak form equations with different continuity requirements: fourth-order derivatives for HSDT-4 and HSDT-5 and third-order derivatives for HSDT-7. Notably, HSDT-4 achieves no reduction in derivative order compared to HSDT-5 despite introducing one only reduced variable, whereas HSDT-7 lowers the continuity requirement by one order while adding two extra unknowns. These varying combinations of derivative order and number of variable show different computational challenges. The elevated continuity demands create a critical challenge for standard numerical discretization schemes. However, NURBS basis functions

Table 3
The first dimensionless natural frequency of the simply supported FG-MEE square nanoplates for varying l, μ and n) (fixed parameters: $L = 10$, $L/t = 10$).

μ	l	Theories	n			
			1	2	5	10
0	0	HSDT-4	4.0040	3.9268	3.8535	3.8020
		HSDT-5	4.0040	3.9268	3.8535	3.8020
		HSDT-7	4.0040	3.9268	3.8535	3.8020
		HSDT-7 [74]	4.0040	3.9268	3.8535	3.8020
	0.5	HSDT-4	4.0282	3.9503	3.8764	3.8244
		HSDT-5	4.0223	3.9447	3.8711	3.8194
		HSDT-7	4.1015	4.0224	3.9473	3.8945
		HSDT-7 [74]	4.1014	4.0223	3.9473	3.8945
	1	HSDT-4	4.0976	4.0178	3.9423	3.8891
		HSDT-5	4.0769	3.9981	3.9236	3.8710
		HSDT-7	4.3798	4.2953	4.2151	4.1588
		HSDT-7 [74]	4.3794	4.2949	4.2147	4.1584
0.5	0	HSDT-4	3.9087	3.8334	3.7618	3.7115
		HSDT-5	3.9087	3.8334	3.7618	3.7115
		HSDT-7	3.9087	3.8334	3.7618	3.7115
		HSDT-7 [74]	3.9087	3.8333	3.7618	3.7115
	0.5	HSDT-4	3.9323	3.8563	3.7842	3.7334
		HSDT-5	3.9266	3.8509	3.7790	3.7285
		HSDT-7	4.0039	3.9266	3.8534	3.8018
		HSDT-7 [74]	4.0038	3.9266	3.8533	3.8018
	1	HSDT-4	4.0001	3.9221	3.8484	3.7965
		HSDT-5	3.9798	3.9029	3.8302	3.7789
		HSDT-7	4.2755	4.1930	4.1148	4.0598
		HSDT-7 [74]	4.2751	4.1926	4.1144	4.0594
1	0	HSDT-4	3.6591	3.5886	3.5216	3.4745
		HSDT-5	3.6591	3.5886	3.5216	3.4745
		HSDT-7	3.6591	3.5886	3.5216	3.4745
		HSDT-7 [74]	3.6591	3.5886	3.5216	3.4745
	0.5	HSDT-4	3.6812	3.6100	3.5425	3.4950
		HSDT-5	3.6759	3.6050	3.5377	3.4904
		HSDT-7	3.7482	3.6759	3.6073	3.5590
		HSDT-7 [74]	3.7481	3.6759	3.6072	3.5590
	1	HSDT-4	3.7446	3.6717	3.6027	3.5541
		HSDT-5	3.7257	3.6537	3.5856	3.5376
		HSDT-7	4.0024	3.9252	3.8519	3.8004
		HSDT-7 [74]	4.0020	3.9248	3.8515	3.8001

Table 4
The first dimensionless natural frequency of the simply supported FG-MEE square nanoplates for varying l, μ and n) (fixed parameters: $L = 10$, $L/t = 15$).

μ	l	Theories	n			
			1	2	5	10
0	0	HSDT-4	4.0910	4.0091	3.9314	3.8772
		HSDT-5	4.0910	4.0091	3.9314	3.8772
		HSDT-7	4.0910	4.0091	3.9314	3.8772
		HSDT-7 [75]	4.0894	4.0074	3.9298	3.8756
	0.5	HSDT-4	4.1126	4.0300	3.9519	3.8973
		HSDT-5	4.1098	4.0274	3.9494	3.8949
		HSDT-7	4.1906	4.1067	4.0271	3.9716
		HSDT-7 [75]	4.1798	4.0962	4.0169	3.9617
	1	HSDT-4	4.1753	4.0912	4.0117	3.9561
		HSDT-5	4.1655	4.0819	4.0028	3.9476
		HSDT-7	4.4748	4.3852	4.3002	4.2409
		HSDT-7 [75]	4.4631	4.3739	4.2894	4.2305
0.5	0	HSDT-4	3.9937	3.9137	3.8379	3.7850
		HSDT-5	3.9937	3.9137	3.8379	3.7850
		HSDT-7	3.9937	3.9137	3.8378	3.7849
		HSDT-7 [75]	3.9920	3.9120	3.8362	3.7834
	0.5	HSDT-4	4.0147	3.9341	3.8578	3.8046
		HSDT-5	4.0120	3.9316	3.8554	3.8022
		HSDT-7	4.0909	4.0089	3.9313	3.8771
		HSDT-7 [75]	4.0802	3.9986	3.9213	3.8674
	1	HSDT-4	4.0760	3.9938	3.9162	3.8619
		HSDT-5	4.0664	3.9847	3.9076	3.8536
		HSDT-7	4.3683	4.2808	4.1978	4.1400
		HSDT-7 [75]	4.3568	4.2697	4.1872	4.1298
1	0	HSDT-4	3.7387	3.6638	3.5928	3.5433
		HSDT-5	3.7387	3.6638	3.5928	3.5433
		HSDT-7	3.7387	3.6638	3.5928	3.5432
		HSDT-7 [75]	3.7370	3.6621	3.5911	3.5417
	0.5	HSDT-4	3.7583	3.6829	3.6115	3.5616
		HSDT-5	3.7558	3.6805	3.6092	3.5594
		HSDT-7	3.8296	3.7529	3.6802	3.6295
		HSDT-7 [75]	3.8195	3.7431	3.6707	3.6202
	1	HSDT-4	3.8157	3.7388	3.6661	3.6153
		HSDT-5	3.8067	3.7303	3.6581	3.6076
		HSDT-7	4.0893	4.0074	3.9297	3.8756
		HSDT-7 [75]	4.0784	3.9969	3.9197	3.8659

Table 5
The first dimensionless natural frequency of the simply supported FG-MEE square nanoplates for varying l, μ and n) (fixed parameters: $L = 10$, $L/t = 100$).

μ	l	Theories	n			
			1	2	5	10
0	0	HSDT-4	4.1642	4.0782	3.9967	3.9402
		HSDT-5	4.1642	4.0782	3.9967	3.9402
		HSDT-7	4.1642	4.0782	3.9967	3.9402
	0.5	HSDT-4	4.1834	4.0969	4.0150	3.9583
		HSDT-5	4.1833	4.0968	4.0150	3.9582
		HSDT-7	4.2658	4.1776	4.0942	4.0363
	1	HSDT-4	4.2402	4.1523	4.0694	4.0118
		HSDT-5	4.2400	4.1521	4.0692	4.0116
		HSDT-7	4.5534	4.4593	4.3702	4.3084
0.5	0	HSDT-4	4.0651	3.9811	3.9016	3.8465
		HSDT-5	4.0651	3.9811	3.9016	3.8465
		HSDT-7	4.0652	3.9811	3.9016	3.8465
	0.5	HSDT-4	4.0838	3.9994	3.9195	3.8641
		HSDT-5	4.0838	3.9993	3.9194	3.8640
		HSDT-7	4.1643	4.0782	3.9967	3.9403
	1	HSDT-4	4.1393	4.0535	3.9726	3.9163
		HSDT-5	4.1390	4.0533	3.9724	3.9161
		HSDT-7	4.4450	4.3532	4.2662	4.2059
1	0	HSDT-4	3.8055	3.7269	3.6525	3.6008
		HSDT-5	3.8055	3.7269	3.6525	3.6008
		HSDT-7	3.8056	3.7269	3.6525	3.6009
	0.5	HSDT-4	3.8230	3.7440	3.6692	3.6173
		HSDT-5	3.8230	3.7439	3.6691	3.6173
		HSDT-7	3.8983	3.8178	3.7415	3.6886
	1	HSDT-4	3.8750	3.7947	3.7189	3.6662
		HSDT-5	3.8748	3.7945	3.7187	3.6661
		HSDT-7	4.1611	4.0751	3.9938	3.9373

inherently satisfy these high-order smoothness requirements, making isogeometric analysis the natural choice for such formulations.

The electric and magnetic fields are formulated as follows by inserting Eq. (48) into Eq. (35)

$$\widehat{\mathbf{E}}^b = \sum_{I=1}^{m\times n} \widehat{\mathbf{B}}^b_{\varphi I}\mathbf{d}_I;\ \widehat{\mathbf{E}}^s = \sum_{I=1}^{m\times n} \widehat{\mathbf{B}}^s_{\varphi I}\mathbf{d}_I;\ \widehat{\mathbf{H}}^b = \sum_{I=1}^{m\times n} \widehat{\mathbf{B}}^b_{\psi I}\mathbf{d}_I;\ \widehat{\mathbf{H}}^s = \sum_{I=1}^{m\times n} \widehat{\mathbf{B}}^s_{\psi I}\mathbf{d}_I \tag{54}$$

where

$$\text{HSDT}-4:\ \widehat{\mathbf{B}}^b_{\varphi I} = \begin{bmatrix} 0&0&0&0&0&0\\ 0&0&0&0&0&0\\ 0&0&0&0&-R_I&0 \end{bmatrix};\ \widehat{\mathbf{B}}^s_{\varphi I} = \begin{bmatrix} 0&0&0&0&-R_{I,x}&0\\ 0&0&0&0&-R_{I,y}&0 \end{bmatrix}$$
$$\widehat{\mathbf{B}}^b_{\psi I} = \begin{bmatrix} 0&0&0&0&0&0\\ 0&0&0&0&0&0\\ 0&0&0&0&0&-R_I \end{bmatrix};\ \widehat{\mathbf{B}}^s_{\psi I} = \begin{bmatrix} 0&0&0&0&0&-R_{I,x}\\ 0&0&0&0&0&-R_{I,y} \end{bmatrix} \tag{55}$$

$$\text{HSDT}-5:\ \widehat{\mathbf{B}}^b_{\varphi I} = \begin{bmatrix} 0&0&0&0&0&0&0\\ 0&0&0&0&0&0&0\\ 0&0&0&0&0&-R_I&0 \end{bmatrix};\ \widehat{\mathbf{B}}^s_{\varphi I} = \begin{bmatrix} 0&0&0&0&0&-R_{I,x}&0\\ 0&0&0&0&0&-R_{I,y}&0 \end{bmatrix}$$
$$\widehat{\mathbf{B}}^b_{\psi I} = \begin{bmatrix} 0&0&0&0&0&0&0\\ 0&0&0&0&0&0&0\\ 0&0&0&0&0&0&-R_I \end{bmatrix};\ \widehat{\mathbf{B}}^s_{\psi I} = \begin{bmatrix} 0&0&0&0&0&0&-R_{I,x}\\ 0&0&0&0&0&0&-R_{I,y} \end{bmatrix} \tag{56}$$

$$\text{HSDT}-7:\ \widehat{\mathbf{B}}^b_{\varphi I} = \begin{bmatrix} 0&0&0&0&0&0&0&0&0\\ 0&0&0&0&0&0&0&0&0\\ 0&0&0&0&0&0&0&-R_I&0 \end{bmatrix}$$
$$\widehat{\mathbf{B}}^s_{\varphi I} = \begin{bmatrix} 0&0&0&0&0&0&0&-R_{I,x}&0\\ 0&0&0&0&0&0&0&-R_{I,y}&0 \end{bmatrix}$$
$$\widehat{\mathbf{B}}^b_{\psi I} = \begin{bmatrix} 0&0&0&0&0&0&0&0&0\\ 0&0&0&0&0&0&0&0&0\\ 0&0&0&0&0&0&0&0&-R_I \end{bmatrix}$$
$$\widehat{\mathbf{B}}^s_{\psi I} = \begin{bmatrix} 0&0&0&0&0&0&0&0&-R_{I,x}\\ 0&0&0&0&0&0&0&0&-R_{I,y} \end{bmatrix} \tag{57}$$

Substituting Eq. (48) into Eq. (26) yields the components of the displacement fields

$$\widehat{\mathbf{u}} = \left\{ \mathbf{u}^1 \quad \mathbf{u}^2 \quad \mathbf{u}^3 \right\}^T = \sum_{I=1}^{mxn} \left\{ \mathbf{M}^1_I \quad \mathbf{M}^2_I \quad \mathbf{M}^3_I \right\}^T \mathbf{d}_I = \sum_{I=1}^{mxn} \widehat{\mathbf{M}}_I\mathbf{d}_I \tag{58}$$

where

$$\text{HSDT}-4:\ \mathbf{M}^1_I = \begin{bmatrix} R_I&0&0&0&0&0\\ 0&R_I&0&0&0&0\\ 0&0&R_I&R_I&0&0 \end{bmatrix};\ \mathbf{M}^2_I = -\begin{bmatrix} 0&0&R_{I,x}&0&0&0\\ 0&0&R_{I,x}&0&0&0\\ 0&0&0&0&0&0 \end{bmatrix}$$
$$\mathbf{M}^3_I = \begin{bmatrix} 0&0&0&R_{I,x}&0&0\\ 0&0&0&R_{I,x}&0&0\\ 0&0&0&0&0&0 \end{bmatrix} \tag{59}$$

$$\text{HSDT}-5:\ \mathbf{M}^1_I = \begin{bmatrix} R_I&0&0&0&0&0&0\\ 0&R_I&0&0&0&0&0\\ 0&0&R_I&0&0&0&0 \end{bmatrix};\ \mathbf{M}^2_I = -\begin{bmatrix} 0&0&R_{I,x}&0&0&0&0\\ 0&0&R_{I,x}&0&0&0&0\\ 0&0&0&0&0&0&0 \end{bmatrix}$$
$$\mathbf{M}^3_I = \begin{bmatrix} 0&0&0&R_I&0&0&0\\ 0&0&0&0&R_I&0&0\\ 0&0&0&0&0&0&0 \end{bmatrix} \tag{60}$$

Table 6
The first dimensionless natural frequency of the fully clamped FG-MEE square nanoplates with various values of *n, l* and μ ($L = 10$, $L/t = 10$).

μ	l	Theories	n			
			1	2	5	10
0	0	HSDT-4	6.8300	6.7023	6.5820	6.4993
		HSDT-5	6.7666	6.6418	6.5242	6.4432
		HSDT-7	6.7195	6.5921	6.4718	6.3902
		HSDT-7 [74]	6.7198	6.5924	6.4722	6.3904
	0.5	HSDT-4	7.0210	6.8937	6.7731	6.6885
		HSDT-5	7.1218	6.9914	6.8683	6.7812
		HSDT-7	6.8945	6.7654	6.6419	6.5578
		HSDT-7 [74]	6.8946	6.7659	6.6429	6.5581
	1	HSDT-4	7.3396	7.2159	7.0866	6.9955
		HSDT-5	7.3843	7.2584	7.1289	7.0363
		HSDT-7	7.2442	7.0868	6.9569	6.8682
		HSDT-7 [74]	7.2088	7.0827	6.9530	6.8639
0.5	0	HSDT-4	6.6380	6.5139	6.3970	6.3166
		HSDT-5	6.5767	6.4554	6.3411	6.2624
		HSDT-7	6.5343	6.4105	6.2936	6.2142
		HSDT-7 [74]	6.5345	6.4108	6.2940	6.2144
	0.5	HSDT-4	6.8191	6.6953	6.5782	6.4959
		HSDT-5	6.9074	6.7812	6.6621	6.5776
		HSDT-7	6.7165	6.5907	6.4705	6.3885
		HSDT-7 [74]	6.7165	6.5911	6.4714	6.3888
	1	HSDT-4	7.1264	7.0060	6.8804	6.7921
		HSDT-5	7.1565	7.0347	6.9096	6.8202
		HSDT-7	7.0873	6.9332	6.8062	6.7194
		HSDT-7 [74]	7.0521	6.9288	6.8021	6.7150
1	0	HSDT-4	6.1441	6.0293	5.9212	5.8466
		HSDT-5	6.0882	5.9760	5.8702	5.7972
		HSDT-7	6.0561	5.9417	5.8336	5.7599
		HSDT-7 [74]	6.0563	5.9419	5.8339	5.7601
	0.5	HSDT-4	6.3017	6.1872	6.0789	6.0027
		HSDT-5	6.3618	6.2460	6.1370	6.0594
		HSDT-7	6.2530	6.1361	6.0243	5.9479
		HSDT-7 [74]	6.2529	6.1364	6.0251	5.9481
	1	HSDT-4	6.5814	6.4695	5.4625	6.2722
		HSDT-5	6.5795	6.4680	6.3540	6.2723
		HSDT-7	6.6753	6.5297	6.4103	6.3286
		HSDT-7 [74]	6.6406	6.5250	6.4058	6.3238

Table 7
The first dimensionless natural frequency of the fully clamped FG-MEE square nanoplates with various values of *n, l* and μ ($L = 10$, $L/t = 100$).

μ	l	Theories	n			
			1	2	5	10
0	0	HSDT-4	7.5755	7.4174	7.2675	7.1635
		HSDT-5	7.5739	7.4159	7.2661	7.1622
		HSDT-7	7.5732	7.4150	7.2651	7.1611
	0.5	HSDT-4	7.6513	7.4928	7.3429	7.2389
		HSDT-5	7.6532	7.4946	7.3447	7.2406
		HSDT-7	7.7659	7.6045	7.4516	7.3456
	1	HSDT-4	7.8414	7.6784	7.5251	7.4183
		HSDT-5	7.8424	7.6794	7.5260	7.4192
		HSDT-7	7.9444	7.7797	7.6235	7.5156
0.5	0	HSDT-4	7.3579	7.2044	7.0588	6.9578
		HSDT-5	7.3564	7.2030	7.0575	6.9566
		HSDT-7	7.3558	7.2022	7.0566	6.9556
	0.5	HSDT-4	7.4313	7.2773	7.1318	7.0308
		HSDT-5	7.4330	7.2790	7.1334	7.0323
		HSDT-7	7.5598	7.4027	7.2538	7.1507
	1	HSDT-4	7.6163	7.4580	7.3092	7.2054
		HSDT-5	7.6172	7.4588	7.3099	7.2061
		HSDT-7	7.7754	7.6141	7.4612	7.3554
1	0	HSDT-4	6.8004	6.6586	6.5242	6.4310
		HSDT-5	6.7991	6.6574	6.5231	6.4299
		HSDT-7	6.7987	6.6568	6.5224	6.4291
	0.5	HSDT-4	6.8679	6.7256	6.5912	6.4978
		HSDT-5	6.8691	6.7268	6.5923	6.4989
		HSDT-7	7.0256	6.8796	6.7413	6.6454
	1	HSDT-4	7.0398	6.8929	5.0231	6.6600
		HSDT-5	7.0402	6.8939	6.7562	6.6604
		HSDT-7	7.3300	7.1777	7.0334	6.9335

$$\text{HSDT}-7:\ \mathbf{M}_I^1=\begin{bmatrix}R_I&0&0&0&0&0&0&0&0\\0&R_I&0&0&0&0&0&0&0\\0&0&R_I&0&0&0&0&0&0\end{bmatrix}$$
$$\mathbf{M}_I^2=-\begin{bmatrix}0&0&0&0&0&R_I&0&0&0\\0&0&0&0&0&0&R_I&0&0\\0&0&0&0&0&0&0&0&0\end{bmatrix} \quad (61)$$
$$\mathbf{M}_I^3=\begin{bmatrix}0&0&0&R_I&0&0&0&0&0\\0&0&0&0&R_I&0&0&0&0\\0&0&0&0&0&0&0&0&0\end{bmatrix}$$

Similarly, substituting Eq. (48) into Eq. (46) yields the matrix

$$\mathbf{B}^g=\sum_{I=1}^{m\times n}\widehat{\mathbf{B}}_I^g\mathbf{d}_I \quad (62)$$

where

$$\text{HSDT}-4:\ \widehat{\mathbf{B}}_I^g=\begin{bmatrix}0&0&N_{I,x}&N_{I,x}&0&0\\0&0&N_{I,y}&N_{I,y}&0&0\end{bmatrix} \quad (63)$$

$$\text{HSDT}-5:\ \widehat{\mathbf{B}}_I^g=\begin{bmatrix}0&0&N_{I,x}&0&0&0&0\\0&0&N_{I,y}&0&0&0&0\end{bmatrix} \quad (64)$$

$$\text{HSDT}-7:\ \widehat{\mathbf{B}}_I^g=\begin{bmatrix}0&0&N_{I,x}&0&0&0&0&0&0\\0&0&N_{I,y}&0&0&0&0&0&0\end{bmatrix} \quad (65)$$

The final compact form is obtained by substituting the corresponding components into Eq. (47)

$$\left((\mathbf{K}_0+\mathbf{K}_1-\mathbf{K}_g)-\omega^2\mathbf{M}\right)\overline{\mathbf{d}}=\mathbf{0} \quad (66)$$

The system components namely the global stiffness matrix ($\mathbf{K}=\mathbf{K}_0+\mathbf{K}_1$), mass matrix ($\mathbf{M}$) and geometry matrix ($\mathbf{K}_g$) are formulated as

$$\begin{aligned}\mathbf{K}_0=&\int_\Omega(\widehat{\mathbf{B}}^b)^T\widehat{\mathbf{D}}^b_{uu}\widehat{\mathbf{B}}^b\mathrm{d}\Omega-\int_\Omega(\widehat{\mathbf{B}}^b)^T\widehat{\mathbf{D}}^b_{ue}\widehat{\mathbf{B}}^b_\varphi\mathrm{d}\Omega-\int_\Omega(\widehat{\mathbf{B}}^b)^T\widehat{\mathbf{D}}^b_{um}\widehat{\mathbf{B}}^b_\psi\mathrm{d}\Omega\\
&+\int_\Omega(\widehat{\mathbf{B}}^s)^T\widehat{\mathbf{D}}^s_{uu}\widehat{\mathbf{B}}^s\mathrm{d}\Omega-\int_\Omega(\widehat{\mathbf{B}}^s)^T\widehat{\mathbf{D}}^s_{ue}\widehat{\mathbf{B}}^s_\varphi\mathrm{d}\Omega-\int_\Omega(\widehat{\mathbf{B}}^s)^T\widehat{\mathbf{D}}^s_{um}\widehat{\mathbf{B}}^s_\psi\mathrm{d}\Omega\\
&-\int_\Omega(\widehat{\mathbf{B}}^b_\varphi)^T\widehat{\mathbf{D}}^b_{eu}\widehat{\mathbf{B}}^b\mathrm{d}\Omega-\int_\Omega(\widehat{\mathbf{B}}^b_\varphi)^T\widehat{\mathbf{D}}^b_{ee}\widehat{\mathbf{B}}^b_\varphi\mathrm{d}\Omega-\int_\Omega(\widehat{\mathbf{B}}^b_\varphi)^T\widehat{\mathbf{D}}^b_{em}\widehat{\mathbf{B}}^b_\psi\mathrm{d}\Omega\\
&-\int_\Omega(\widehat{\mathbf{B}}^s_\varphi)^T\widehat{\mathbf{D}}^s_{eu}\widehat{\mathbf{B}}^s\mathrm{d}\Omega-\int_\Omega(\widehat{\mathbf{B}}^s_\varphi)^T\widehat{\mathbf{D}}^s_{ee}\widehat{\mathbf{B}}^s_\varphi\mathrm{d}\Omega-\int_\Omega(\widehat{\mathbf{B}}^s_\varphi)^T\widehat{\mathbf{D}}^s_{em}\widehat{\mathbf{B}}^s_\psi\mathrm{d}\Omega\\
&-\int_\Omega(\widehat{\mathbf{B}}^b_\psi)^T\widehat{\mathbf{D}}^b_{mu}\widehat{\mathbf{B}}^b\mathrm{d}\Omega-\int_\Omega(\widehat{\mathbf{B}}^b_\psi)^T\widehat{\mathbf{D}}^b_{me}\widehat{\mathbf{B}}^b_\varphi\mathrm{d}\Omega-\int_\Omega(\widehat{\mathbf{B}}^b_\psi)^T\widehat{\mathbf{D}}^b_{mm}\widehat{\mathbf{B}}^b_\psi\mathrm{d}\Omega\\
&-\int_\Omega(\widehat{\mathbf{B}}^s_\psi)^T\widehat{\mathbf{D}}^s_{mu}\widehat{\mathbf{B}}^s\mathrm{d}\Omega-\int_\Omega(\widehat{\mathbf{B}}^s_\psi)^T\widehat{\mathbf{D}}^s_{me}\widehat{\mathbf{B}}^s_\varphi\mathrm{d}\Omega-\int_\Omega(\widehat{\mathbf{B}}^s_\psi)^T\widehat{\mathbf{D}}^s_{mm}\widehat{\mathbf{B}}^s_\psi\mathrm{d}\Omega\end{aligned}$$

$$\mathbf{K}_g=\int_\Omega(1-\mu^2\nabla^2)(\widehat{\mathbf{B}}^g)^T\begin{bmatrix}N_x^{elec}+N_x^{mag}&0\\0&N_y^{elec}+N_y^{mag}\end{bmatrix}\widehat{\mathbf{B}}^g\mathrm{d}\Omega$$

$$\mathbf{M}=\int_\Omega(1-\mu^2\nabla^2)\widehat{\mathbf{M}}^T\widehat{\mathbf{I}}_m\widehat{\mathbf{M}}\mathrm{d}\Omega;\ \mathbf{d}=\overline{\mathbf{d}}e^{i\omega t} \quad (67)$$

here ω is the natural frequency and $\overline{\mathbf{d}}$ is the corresponded mode shapes.

3. Numerical examples

This section examines the natural frequencies of FG-MEE square nanoplates with side length L and thickness t. Two boundary conditions are considered: simply supported and fully clamped. The investigation is conducted by comparing three distinct higher-order shear deformation theory (HSDT) models. For all numerical examples, the domain is discretized using a 13 × 13 mesh of cubic NURBS elements. Material properties are tabulated in Table 1. The dimensionless natural frequencies are normalized by $\overline{\omega}=\omega L^2/t\sqrt{\rho_c/c_{11c}}$, in which c represents the $CoFe_2O_4$ material. The nonlocal strain gradient theory is a generalized model that incorporates both nonlocal and strain gradient effects. This theory reduces to the pure nonlocal theory when the strain gradient parameter (l) is set to zero or to the pure strain gradient theory when the nonlocal parameter (μ) is set to zero, respectively. As a special case, the model recovers the classical continuum theory when both size-effect parameters (nonlocal and strain gradient) are neglected. To easily compare HSDT models, the applied electric voltage and magnetic potentials are set to zero (V_0 =0, $\Omega_0=0$). The boundary conditions for HSDT-4, HSDT-5, HSDT-7 models are tabulated in Table 2.

Table 2 gives boundary conditions for numerical examples. HSDT-7 easily enforces these constraints that directly set all kinematic variables to zero, however, HSDT-4 and HSDT-5 introduce a different challenge for fully clamped boundary conditions. These theories cannot directly impose the slope constraints because the necessary rotational derivatives do not appear as independent variables. They are completely absent in the respective kinematic fields, which complicates the boundary condition implementation. It is observed that HSDT-7 easily imposes boundary conditions when comparing to HSDT-4 and HSDT-5. However, IGA offers a notably simpler approach for enforcing derivative boundary conditions [73]. To impose the constraint on $\frac{\partial w^b}{\partial n},\frac{\partial w^s}{\partial n},\frac{\partial w}{\partial n}$, we apply identical boundary values (for instance, zero) to both the boundary control points and their immediately adjacent interior control points. This technique is substantially more straightforward to implement in the IGA framework compared to alternative numerical methods.

Firstly, the influence of various parameters including length-to-thickness ratios, power-law indexes, control parameters, boundary conditions and HSDTs on the first dimensionless natural frequency of simply supported FG-MEE nanoplates is studied and tabulated in

$$\begin{aligned}\mathbf{K}_1=&-l^2\int_\Omega(\widehat{\mathbf{B}}^b)^T\widehat{\mathbf{D}}^b_{uu}\nabla^2\widehat{\mathbf{B}}^b\mathrm{d}\Omega+l^2\int_\Omega(\widehat{\mathbf{B}}^b)^T\widehat{\mathbf{D}}^b_{ue}\nabla^2\widehat{\mathbf{B}}^b_\varphi\mathrm{d}\Omega+l^2\int_\Omega(\widehat{\mathbf{B}}^b)^T\widehat{\mathbf{D}}^b_{um}\nabla^2\widehat{\mathbf{B}}^b_\psi\mathrm{d}\Omega\\
&-l^2\int_\Omega(\widehat{\mathbf{B}}^s)^T\widehat{\mathbf{D}}^s_{uu}\nabla^2\widehat{\mathbf{B}}^s\mathrm{d}\Omega+l^2\int_\Omega(\widehat{\mathbf{B}}^s)^T\widehat{\mathbf{D}}^s_{ue}\nabla^2\widehat{\mathbf{B}}^s_\varphi\mathrm{d}\Omega+l^2\int_\Omega(\widehat{\mathbf{B}}^s)^T\widehat{\mathbf{D}}^s_{um}\nabla^2\widehat{\mathbf{B}}^s_\psi\mathrm{d}\Omega\\
&+l^2\int_\Omega(\widehat{\mathbf{B}}^b_\varphi)^T\widehat{\mathbf{D}}^b_{eu}\nabla^2\widehat{\mathbf{B}}^b\mathrm{d}\Omega+l^2\int_\Omega(\widehat{\mathbf{B}}^b_\varphi)^T\widehat{\mathbf{D}}^b_{ee}\nabla^2\widehat{\mathbf{B}}^b_\varphi\mathrm{d}\Omega+l^2\int_\Omega(\widehat{\mathbf{B}}^b_\varphi)^T\widehat{\mathbf{D}}^b_{em}\nabla^2\widehat{\mathbf{B}}^b_\psi\mathrm{d}\Omega\\
&+l^2\int_\Omega(\widehat{\mathbf{B}}^s_\varphi)^T\widehat{\mathbf{D}}^s_{eu}\nabla^2\widehat{\mathbf{B}}^s\mathrm{d}\Omega+l^2\int_\Omega(\widehat{\mathbf{B}}^s_\varphi)^T\widehat{\mathbf{D}}^s_{ee}\nabla^2\widehat{\mathbf{B}}^s_\varphi\mathrm{d}\Omega+l^2\int_\Omega(\widehat{\mathbf{B}}^s_\varphi)^T\widehat{\mathbf{D}}^s_{em}\nabla^2\widehat{\mathbf{B}}^s_\psi\mathrm{d}\Omega\\
&+l^2\int_\Omega(\widehat{\mathbf{B}}^b_\psi)^T\widehat{\mathbf{D}}^b_{mu}\nabla^2\widehat{\mathbf{B}}^b\mathrm{d}\Omega+l^2\int_\Omega(\widehat{\mathbf{B}}^b_\psi)^T\widehat{\mathbf{D}}^b_{me}\nabla^2\widehat{\mathbf{B}}^b_\varphi\mathrm{d}\Omega+l^2\int_\Omega(\widehat{\mathbf{B}}^b_\psi)^T\widehat{\mathbf{D}}^b_{mm}\nabla^2\widehat{\mathbf{B}}^b_\psi\mathrm{d}\Omega\\
&+l^2\int_\Omega(\widehat{\mathbf{B}}^s_\psi)^T\widehat{\mathbf{D}}^s_{mu}\nabla^2\widehat{\mathbf{B}}^s\mathrm{d}\Omega+l^2\int_\Omega(\widehat{\mathbf{B}}^s_\psi)^T\widehat{\mathbf{D}}^s_{me}\nabla^2\widehat{\mathbf{B}}^s_\varphi\mathrm{d}\Omega+l^2\int_\Omega(\widehat{\mathbf{B}}^s_\psi)^T\widehat{\mathbf{D}}^s_{mm}\nabla^2\widehat{\mathbf{B}}^s_\psi\mathrm{d}\Omega\end{aligned}$$

Tables 3–5. The obtained results for simply supported plates are validated against those from Thai et al. [74] (using a seven-variable theory with IGA of 11 × 11 mesh of cubic NURBS elements) and Thai et al. [75] (using the same theory with a meshfree method). As a first validation, the size-effect parameters are set to zero to recover the classical theory. In this limit, the predictions from all three HSDT models (HSDT-4, HSDT-5, HSDT-7) converge to identical values, which are in excellent agreement with the reference findings [74]. The validation study confirms that three HSDTs provide a reliable and accurate framework for modeling the vibrational behavior of FG-MEE plates. In addition, the analysis reduces to the pure nonlocal theory ($\mu \neq 0$ and $l = 0$). HSDT-4, HSDT-5, and HSDT-7 yield perfectly identical predictions when increasing the nonlocal parameter. Therefore, the pure nonlocal theory produces no variations among these three specific HSDT models. All models converge to the identical values from reference [74]. Therefore, it is perfectly suited for this specific case because the HSDT-4 model contains the fewest variables. However, in the case of the pure strain gradient theory ($\mu = 0$ and $l \neq 0$), a divergence between the three HSDT models is observed. The predicted values for the dimensionless natural frequency follow a clear descending order: $\overline{\omega}_{HSDT-7} > \overline{\omega}_{HSDT-4} > \overline{\omega}_{HSDT-5}$. We consider the original HSDT-5 model. HSDT-4 and HSDT-7 represent its derived variants. HSDT-4 and HSDT-5 yield slightly different results. However, this difference remains completely insignificant. HSDT-7 consistently provides the highest frequency. Eq. (33) introduces an additional shear term (ε^{s1}) for this specific model. The pure strain gradient theory actively amplifies this shear term's value. Eqs. (36) and (39) explicitly demonstrate this numerical increase. These specific mathematical formulations define the core differences among the theoretical models. Moreover, based on the preceding observations, we can conclude that the divergence observed between the HSDT models is driven exclusively by the strain gradient effects. The models are shown to be in perfect agreement under pure nonlocal theory, isolating the strain gradient component as the source of the discrepancy.

Consequently, these single-parameter models are often insufficient. They are inherently unidirectional: pure nonlocal theory can only predict stiffness-softening, while pure strain gradient theory can only predict stiffness-hardening. This is a critical limitation, as experimental observations at the nanoscale show a complex, size-dependent reality that can include both hardening and softening behaviors. Additionally, the full nonlocal strain gradient theory (NSGT) reveals a clear competition between the stiffness-softening (nonlocal) and stiffness-hardening (strain gradient) effects. By including both parameters, it can successfully capture the complex crossover behavior that is physically observed at the nanoscale. Under the full NSGT, the dimensionless natural frequency decreases with the nonlocal parameter (μ) but increases with the strain gradient parameter (l). Again, the dimensionless natural frequency values follow a strict descending order. This specific sequence is $\overline{\omega}_{HSDT-7} > \overline{\omega}_{HSDT-4} > \overline{\omega}_{HSDT-5}$. Besides, this competition results in a net softening effect ($\overline{\omega} < \overline{\omega}_{classical}$) when $l \leq \mu$ and a net hardening effect ($\overline{\omega} > \overline{\omega}_{classical}$) when $l > \mu$. We observe a distinct physical interaction from the results. The NSGT model affects the individual HSDT models exclusively through its strain gradient terms. The pure nonlocal components produce completely uniform effects across all models.

Furthermore, the dimensionless natural frequency decreases when the power-law index increases. It is seen that an increase in n shifts the material composition toward the softer bottom surface ($BaTiO_3$). This material shift significantly reduces the effective bending stiffness, leading to a decrease in natural frequency. Moreover, the dimensionless natural frequency increases with a rise of the length-to-thickness ratio. A larger a/h ratio indicates a thinner plate, in which transverse shear deformation is negligible. Additionally, the frequency is significantly amplified by both mathematical normalization process and the nanoscopic strain gradient that heavily stiffens the structure. Consequently, these combined factors strongly lead the dimensionless frequency upward.

While the fully clamped plates exhibit higher natural frequencies due to their increased structural stiffness, the qualitative trends such as the influence of the power-law index, length-to-thickness ratio and size-effect parameters are consistent with those observed for the simply supported boundaries, tabulated in Tables 6 and 7. This study compares three HSDT models to evaluate their trade-off between cost and implementation (boundary conditions), particularly for fully clamped boundaries. The computationally efficient HSDT-4 and HSDT-5 models require high-order derivatives (second-order for two classical HSDT models, fourth-order for NSGT model). This means fully clamped conditions must be enforced on both displacements and their derivatives, a task that is notoriously difficult for most numerical methods. In contrast, the HSDT-7 model is designed to solve this disadvantage. It adds two variables to reformulate the problem, which reduces the derivative order (to first-order for classical HSDT model, third-orderfor NSGT model). While this increases computational cost, it simplifies implementation, as boundary conditions can be applied directly to the primary variables. This study provides a practical guide to balance between computational cost and numerical complexity.

4. Conclusions

This study successfully implemented a robust isogeometric analysis (IGA) approach to investigate the free vibration of FG-MEE nanoplates under the coupled influence of NSGT and HSDTs. The IGA methodology, defined by the inherent high-order continuity of its NURBS basis functions, proved highly effective for overcoming the challenge of implementing NSGT in its weak form. This approach successfully managed the high-order derivative requirements, which enabled a direct implementation without mixed formulations. Specifically, it handled fourth-order derivatives for C^1 theories (HSDT-4, HSDT-5) and third-order derivatives for the C^0 theory (HSDT-7).

The primary conclusions of this investigation are as following:

- ✓ The IGA formulations for all three HSDT models (HSDT-4, HSDT-5, and HSDT-7) were successfully validated. The HSDT models showed excellent agreement with published data for the classical limit ($l = 0$ and $\mu = 0$) and the pure nonlocal case ($l = 0$ and $\mu \neq 0$). Three HSDT models converged to identical predictions. This specific convergence confirmed the accuracy of the present approach.
- ✓ A key finding of this study is that HSDT selection is a critical factor at the nanoscale. While the models converged identically under classical and pure nonlocal conditions, they diverged significantly when pure strain gradient effects were active ($l \neq 0$ and $\mu = 0$), with frequencies following ($\overline{\omega}_{HSDT-7} > \overline{\omega}_{HSDT-4} > \overline{\omega}_{HSDT-5}$). This demonstrates conclusively that the discrepancy between HSDT models was driven exclusively by the strain gradient components.
- ✓ Three HSDT models presented distinct trade-offs between computational cost and numerical complexity. HSDT-4 and HSDT-5 are computationally efficient but require fourth-order derivative in approximated formulations, which complicates in enforcing fully clamped conditions since slope constraints cannot be directly imposed. Conversely, HSDT-7 introduces two additional variables that reduce the NSGT derivative requirements to third-order, which enables the direct enforcement of boundary conditions
- ✓ The study confirmed the power of the two-parameter NSGT in capturing competing nanoscale physics. A net stiffness-softening effect ($\overline{\omega} < \overline{\omega}_{classical}$) was observed when the nonlocal influence dominates ($l \leq \mu$). Conversely, a net stiffness-hardening effect ($\overline{\omega} > \overline{\omega}_{classical}$) was occurred when the strain gradient parameter dominates ($l > \mu$). This dual-parameter capability enables reproduction of experimentally observed crossover behaviors that single-parameter models cannot capture.
- ✓ The parametric study demonstrated consistent qualitative trends across all HSDTs and boundary conditions. The natural frequency decreased with increasing power-law index (due to a softer material

composition) and increased with increasing length-to-thickness ratio.

In conclusion, this work provides a robust computational approach for analyzing FG-MEE nanoplates. It demonstrates that the IGA-based solution not only makes computationally efficient models (like HSDT-4 and HSDT-5) viable but also provides a platform to accurately quantify the differences between these advanced theories. The results establish HSDT selection as a governing determinant in nanoscale multiphysics analysis, which is fundamentally essential for the accurate design and optimization of MEE nanodevices.

CRediT authorship contribution statement

Chien H. Thai: Writing – original draft, Visualization, Validation, Methodology, Investigation, Formal analysis, Conceptualization. **P.T. Hung:** Writing – review & editing, Visualization, Validation, Investigation. **Magd Abdel Wahab:** Writing – review & editing, Visualization, Validation. **P. Phung-Van:** Writing – review & editing, Visualization, Validation, Methodology, Investigation, Conceptualization.

Declaration of competing interest

The authors declare that they have no known competing financial interests or personal relationships that could have appeared to influence the work reported in this paper.

Data availability

No data was used for the research described in the article.

References

[1] Torkashvand Z, Shayeganfar F, Ramazani A. Nanomaterials based micro/nanoelectromechanical system (MEMS and NEMS) devices. Micromach (Basel) 2024.
[2] Elnaggar A, Kang S, Tian M, Han B, Keshavarz M. State of the art in actuation of micro/nanorobots for biomedical applications. Small Sci 2024;4(3):2300211.
[3] Thai H-T, Vo TP, Nguyen T-K, Kim S-E. A review of continuum mechanics models for size-dependent analysis of beams and plates. Compos Struct 2017;177:196–219.
[4] Zheng H, Wang J, Lofland SE. Multiferroic BaTiO3-CoFe2O4 nanostructures. Science 2004:303.
[5] Martin LW, Crane SP, Chu YH. Multiferroics and magnetoelectrics: thin films and nanostructures. J Phys: Condens Matter 2008;20.
[6] Zhou L, Ren S, Nie B, Guo G, Cui X-Y. Coupling Magneto-Electro-Elastic node-based smoothed radial point interpolation method for free vibration and transient analysis of functionally graded Magneto-Electro-Elastic structures. Chin J Aeronaut 2019:33.
[7] Will-Cole A, Hassanien A, Calisgan S, Jeong M-G, Liang X, Kang S, et al. Tutorial: piezoelectric and magnetoelectric N/MEMS—materials, devices, and applications. J Appl Phys 2022;131:241101.
[8] Desai S, Sidhardh S. Beyond classical elasticity: a review of strain gradient theories, emphasizing computer modeling, physical interpretations, and multifunctional applications. CMES - Comput Model Eng Sci 2025;144(2):1271–334.
[9] Lam DCC, Yang F, Chong ACM, Wang J, Tong P. Experiments and theory in strain gradient elasticity. J Mech Phys Solids 2003;51(8):1477–508.
[10] Yang F, Chong ACM, Lam DCC, Tong P. Couple stress based strain gradient theory for elasticity. Int J Solid Struct 2002;39(10):2731–43.
[11] Lim CW, Zhang G, Reddy JN. A higher-order nonlocal elasticity and strain gradient theory and its applications in wave propagation. J Mech Phys Solid 2015;78:298–313.
[12] Jafari A, Shirvani Shah-enayati S, Atai AA. Size dependency in vibration analysis of nano plates; one problem, different answers. Eur J Mech - A/Solid 2016;59:124–39.
[13] Challamel N, Wang CM, Reddy JN, Faghidian SA. Equivalence between micromorphic, nonlocal gradient, and two-phase nonlocal beam theories. Acta Mech 2025;236(2):871–902.
[14] Faghidian SA, Żur KK, Rabczuk T. Mixture unified gradient theory: a consistent approach for mechanics of nanobars. Eng Anal Bound Elem 2022;128(11):996.
[15] Faghidian SA, Elishakoff I. A consistent approach to characterize random vibrations of nanobeams. Eng Anal Bound Elem 2023;152:14–21.
[16] Reddy JN. A simple higher-order theory for laminated composite plates. J Appl Mech 1984;51(4):745–52.
[17] Whitney JM, Pagano NJ. Shear deformation in heterogeneous anisotropic plates. J Appl Mech 1970;37(4):1031–6.
[18] Levinson M. An accurate, simple theory of the statics and dynamics of elastic plates. Mech Res Commun 1980;7(6):343–50.
[19] Aydogdu M. A new shear deformation theory for laminated composite plates. Compos Struct 2009;89(1):94–101.
[20] Karama M, Afaq KS, Mistou S. Mechanical behaviour of laminated composite beam by the new multi-layered laminated composite structures model with transverse shear stress continuity. Int J Solid Struct 2003;40(6):1525–46.
[21] Thai CH, Ferreira AJM, Bordas SPA, Rabczuk T, Nguyen-Xuan H. Isogeometric analysis of laminated composite and sandwich plates using a new inverse trigonometric shear deformation theory. Eur J Mech - A/Solid 2014;43:89–108.
[22] Chen W, Lee KY, Ding H. On free vibration of non-homogeneous transversely isotropic magneto-electro-elastic plates. J Sound Vib 2005;279(1–2):237–51.
[23] Pan E, Han F. Exact solution for functionally graded and layered magneto-electro-elastic plates. Int J Eng Sci 2005;43(3–4):321–39.
[24] Zhang P, Qi C, Fang H, Ma C, Huang Y. Semi-analytical analysis of static and dynamic responses for laminated magneto-electro-elastic plates. Compos Struct 2019;222:110933.
[25] Liu M.-F., Chang T.-P. Closed form expression for the vibration problem of a transversely isotropic magneto-electro-elastic plate. 2010.
[26] Liu M-F. Exact solution for the bending deformations of layered magneto-electro-elastic laminates based on thin-plate formulation. Int J Eng Appl Sci 2016;3(4):257692.
[27] Ke L-L, Wang Y-S, Yang J, Kitipornchai S. Free vibration of size-dependent magneto-electro-elastic nanoplates based on the nonlocal theory. Acta Mech. Sinica 2014;30(4):516–25.
[28] Jafarsadeghi-pournaki I, Fakhari M, Amiri A, Rezazadeh G. Vibration analysis of circular magneto-electro-elastic nano-plates based on eringen s nonlocal theory. Int J Eng 2015;28(12):1808–17.
[29] Jamalpoor A, Ahmadi-Savadkoohi A, Hosseini M, Hosseini-Hashemi S. Free vibration and biaxial buckling analysis of double magneto-electro-elastic nanoplate-systems coupled by a visco- pasternak medium via nonlocal elasticity theory. Eur J Mech - A/Solid 2017;63:84–98.
[30] Esen I, Özmen R. Thermal vibration and buckling of magneto-electro-elastic functionally graded porous nanoplates using nonlocal strain gradient elasticity. Compos Struct 2022;296:115878.
[31] Chen H, Yu W. A multiphysics model for magneto-electro-elastic laminates. Eur J Mech - A/Solid 2014;47:23–44.
[32] Milazzo A. Large deflection of magneto-electro-elastic laminated plates. Appl Math Model 2014;38(5):1737–52.
[33] Alaimo A, Benedetti I, Milazzo A. A finite element formulation for large deflection of multilayered magneto-electro-elastic plates. Compos Struct 2014;107:643–53.
[34] Mohammadimehr M, Rostami R. Bending, buckling, and forced vibration analyses of nonlocal nanocomposite microplate using TSDT considering MEE properties dependent to various volume fractions of $CoFe_2O_4$-$BaTiO_3$. J Theoret Appl Mech 2017;55.
[35] Vinyas M, Kattimani SC. Finite element evaluation of free vibration characteristics of magneto-electro-elastic rectangular plates in hygrothermal environment using higher-order shear deformation theory. Compos Struct 2018;202:1339–52.
[36] Vinyas M. A higher-order free vibration analysis of carbon nanotube-reinforced magneto-electro-elastic plates using finite element methods. Composites Part B: Engineering 2019;158:286–301.
[37] Mahesh V, Harursampath D. Nonlinear vibration of functionally graded magneto-electro-elastic higher order plates reinforced by CNTs using FEM. Eng Comput 2020:1–23.
[38] Zheng Y-f, Xu L-l, Chen C-p. Nonlinear bending analysis of magnetoelectroelastic rectangular plates using higher order shear deformation theory. J Mech Sci Technol 2021;35(3):1099–108.
[39] Xu LL, Kang CC, Zheng YF, Chen CP. Analysis of nonlinear vibration of magneto-electro-elastic plate on elastic foundation based on high-order shear deformation. Compos Struct 2021;271:114149.
[40] Żur KK, Arefi M, Kim J, Reddy JN. Free vibration and buckling analyses of magneto-electro-elastic FGM nanoplates based on nonlocal modified higher-order sinusoidal shear deformation theory. Compos Part B: Eng 2020;182:107601.
[41] Gholami R, Ansari R. A unified nonlocal nonlinear higher-order shear deformable plate model for postbuckling analysis of piezoelectric-piezomagnetic rectangular nanoplates with various edge supports. Compos Struct 2017;166:202–18.
[42] Malikan M, Nguyen VB. Buckling analysis of piezo-magnetoelectric nanoplates in hygrothermal environment based on a novel one variable plate theory combining with higher-order nonlocal strain gradient theory. Phys E: Low-Dimens Syst Nanostruct 2018;102:8–28.
[43] Vinyas M, Harursampath D. Nonlinear vibrations of magneto-electro-elastic doubly curved shells reinforced with carbon nanotubes. Compos Struct 2020;253:112749.
[44] Mahesh V. Nonlinear pyrocoupled deflection of viscoelastic sandwich shell with CNT reinforced magneto-electro-elastic facing subjected to electromagnetic loads in thermal environment. Eur Phys J Plus 2021;136(8):1–30.
[45] Mahesh V, Harursampath D. Nonlinear deflection analysis of CNT/magneto-electro-elastic smart shells under multi-physics loading. Mech Adv Mater Struct 2022;29(7):1047–71.
[46] Mohammadimehr M, Okhravi S, Akhavan Alavi S. Free vibration analysis of magneto-electro-elastic cylindrical composite panel reinforced by various distributions of CNTs with considering open and closed circuits boundary conditions based on FSDT. J Vibrat Control 2018;24(8):1551–69.
[47] Hughes TJR, Cottrell JA, Bazilevs Y. Isogeometric analysis: CAD, finite elements, NURBS, exact geometry and mesh refinement. Comput Method Appl Mech Eng 2005;194(39):4135–95.

[48] Cottrell JA, Reali A, Bazilevs Y, Hughes TJR. Isogeometric analysis of structural vibrations. Comput Method Appl Mech Eng 2006;195(41):5257–96.
[49] Kiendl J, Auricchio F, Hughes TJR, Reali A. Single-variable formulations and isogeometric discretizations for shear deformable beams. Comput Method Appl Mech Eng 2015;284:988–1004.
[50] Niiranen J, Kiendl J, Niemi AH, Reali A. Isogeometric analysis for sixth-order boundary value problems of gradient-elastic Kirchhoff plates. Comput Method Appl Mech Eng 2017;316:328–48.
[51] Benson DJ, Bazilevs Y, Hsu MC, Hughes TJR. Isogeometric shell analysis: the Reissner–Mindlin shell. Comput Method Appl Mech Eng 2010;199(5):276–89.
[52] Benson DJ, Bazilevs Y, Hsu MC, Hughes TJR. A large deformation, rotation-free, isogeometric shell. Comput Method Appl Mech Eng 2011;200(13):1367–78.
[53] Kiendl J, Bletzinger KU, Linhard J, Wüchner R. Isogeometric shell analysis with Kirchhoff–Love elements. Comput Method Appl Mech Eng 2009;198(49):3902–14.
[54] Nguyen HX, Nguyen TN, Abdel-Wahab M, Bordas SPA, Nguyen-Xuan H, Vo TP. A refined quasi-3D isogeometric analysis for functionally graded microplates based on the modified couple stress theory. Comput Method Appl Mech Eng 2017;313: 904–40.
[55] Thai CH, Ferreira AJM, Tran TD, Phung-Van P. A size-dependent quasi-3D isogeometric model for functionally graded graphene platelet-reinforced composite microplates based on the modified couple stress theory. Compos Struct 2019: 111695.
[56] Thai CH, Ferreira AJM. Nguyen-Xuan H. Isogeometric analysis of size-dependent isotropic and sandwich functionally graded microplates based on modified strain gradient elasticity theory. Compos Struct 2018;192:274–88.
[57] Thai CH, Ferreira AJM, Phung-Van P. Size dependent free vibration analysis of multilayer functionally graded GPLRC microplates based on modified strain gradient theory. Compos Part B-Eng 2019;169:174–88.
[58] Phung-Van P, Thai CH, Abdel-Wahab M, Nguyen-Xuan H. Optimal design of FG sandwich nanoplates using size-dependent isogeometric analysis. Mech Mater 2020;142:103277.
[59] Phung-Van P, Lieu QX, Nguyen-Xuan H, Abdel Wahab M. Size-dependent isogeometric analysis of functionally graded carbon nanotube-reinforced composite nanoplates. Compos Struct 2017;166:120–35.
[60] Phung-Van P, Ferreira AJM, Nguyen-Xuan H, Abdel Wahab M. An isogeometric approach for size-dependent geometrically nonlinear transient analysis of functionally graded nanoplates. Compos Part B: Eng 2017;118:125–34.
[61] Thai CH, Ferreira AJM, Phung-Van P. A nonlocal strain gradient isogeometric model for free vibration and bending analyses of functionally graded plates. Compos Struct 2020;251:112634.
[62] Phung-Van P JM, Ferreira A, Nguyen-Xuan H, Thai CH. Scale-dependent nonlocal strain gradient isogeometric analysis of metal foam nanoscale plates with various porosity distributions. Compos Struct 2021:113949.
[63] Ebrahimi F, Barati MR. Vibration analysis of embedded biaxially loaded magneto-electrically actuated inhomogeneous nanoscale plates. J Vibrat Control 2018;24 (16):3587–607.
[64] Aifantis EC. Update on a class of gradient theories. Mech. Mater 2003;35(3): 259–80.
[65] Arefi M, Kiani M, Zamani MH. Nonlocal strain gradient theory for the magneto-electro-elastic vibration response of a porous FG-core sandwich nanoplate with piezomagnetic face sheets resting on an elastic foundation. J Sandw Struct Mater 2018;22:109963621879537.
[66] Eringen AC. Nonlocal polar elastic continua. Int J Eng Sci 1972;10(1):1–16.
[67] Lu P, Zhang PQ, Lee HP, Wang CM, Reddy JN. Non-local elastic plate theories. Proceed Roy Soc A: Math Phys Eng Sci 2007;463(2088):3225–40.
[68] Senthilnathan N, Lim S, Lee K, ST C. Buckling of shear-deformable plates. AIAA J 1987;25(9):1268–71.
[69] Thai CH, Phung-Van P. A meshfree approach using naturally stabilized nodal integration for multilayer FG GPLRC complicated plate structures. Eng Anal Bound Elem 2020;117:346–58.
[70] Thai CH, Hung PT, Rabczuk T, Nguyen-Xuan H, Phung-Van P. A Chebyshev shear deformation model for laminated composite plates. Compos Struct 2025;360: 119045.
[71] Phung-Van P, Hung PT, Tangaramvong S, Nguyen-Xuan H, Thai CH. A novel Chebyshev-based both meshfree method and shear deformation theory for functionally graded triply periodic minimal surface flat plates. Comput Struct 2025;309:107660.
[72] Ebrahimi F, Barati MR. Static stability analysis of smart magneto-electro-elastic heterogeneous nanoplates embedded in an elastic medium based on a four-variable refined plate theory. Smart Mater Struct 2016;25(10):105014.
[73] Auricchio F, da Veiga LB, Buffa A, Lovadina C, Reali A, Sangalli G. A fully "locking-free" isogeometric approach for plane linear elasticity problems: a stream function formulation. Comput Method Appl Mech Eng 2007;197(1):160–72.
[74] Thai CH, Fereira AMJ, Nguyen-Xuan H, Hung PT, Phung-Van P. A nonlocal strain gradient isogeometric model for free vibration analysis of magneto-electro-elastic functionally graded nanoplates. Compos Struct 2023;316:117005.
[75] Thai CH, Hung PT, Nguyen-Xuan H, Phung-Van P. A size-dependent meshfree approach for magneto-electro-elastic functionally graded nanoplates based on nonlocal strain gradient theory. Eng Struct 2023;292:116521.